REVIEW ARTICLE

WILEY

Structural modulation and assembling of metal halide perovskites for solar cells and light-emitting diodes

Xixia Liu[1,2] | Zhaofu Zhang[3] (iD) | Fen Lin[4] | Yuanhang Cheng[4] (iD)

[1]Department of Materials Science and Engineering, National University of Singapore, Singapore

[2]Department of Materials Science and Engineering, College of Engineering, Peking University, Beijing, China

[3]Department of Engineering, University of Cambridge, Cambridge, UK

[4]Solar Energy Research Institute of Singapore, National University of Singapore, Singapore

Correspondence
Xixia Liu, Department of Materials Science and Engineering, National University of Singapore, Singapore 117576, Singapore.
Email: xixia.liu@u.nus.edu

Yuanhang Cheng, Solar Energy Research Institute of Singapore, National University of Singapore, Singapore 117574, Singapore.
Email: yuancheng9-c@my.cityu.edu.hk

Abstract

Metal halide perovskites possess appealing optoelectronic properties and have been widely applied for solar energy harvesting and light emitting. Although perovskite solar cells (PeSCs) and perovskite light-emitting diodes (PeLEDs) have been developed rapidly in recent years, there are still no universal rules for the selection of perovskites to achieve high-performance optoelectronic devices. In this review, the working mechanisms of PeSCs and PeLEDs are first demonstrated with the discussion on the factors which determine the device performance. We then examine the optoelectronic properties of perovskites with structures modulated from 3D, 2D, 1D to 0D, and analyze the corresponding structure-property relationships in terms of photo-electric and electric-photo conversion processes. Based on the unique optoelectronic properties of structurally modulated perovskites, we put forward the concept of structural assembling engineering that integrate the merits of different types of perovskites within one matrix and elaborate their excellent properties for applications of both PeSCs and PeLEDs. Finally, we discuss the potential challenges and provide our perspectives on the structural assembling engineering of perovskites for future optoelectronic applications.

KEYWORDS
light-emitting diodes, low-dimensional perovskites, metal halide perovskites, solar cells, structural assembling, structure modulation

1 | INTRODUCTION

Metal halide perovskite materials possess appealing properties such as adjustable bandgap in a panchromatic range, the direct transition between photons and charge carriers, high charge carrier mobility, and decent defect tolerance along with low-cost solution-processable techniques.[1] Thanks to these outstanding properties, metal halide perovskites have exhibited great potential to act as both the light absorber and the light-emitting media for optoelectronic applications.[2] For example, the record power conversion efficiency (PCE) of perovskite

solar cells (PeSCs) have been rapidly improved to 25.5%[3] within one decade from 3.8%.[4] Such high PCE of PeSCs has surpassed that of multi-crystalline silicon solar cells (Si-SCs) of 22.8%, and is approaching that of single-crystalline Si-SCs (26.6%) and the single-crystalline GaAs solar cells (27.8%).[5] Concurrently, the development of PeSCs stimulates the evolution of perovskite light-emitting diodes (PeLEDs). The external quantum efficiency (EQE) of PeLEDs have increased to 23.4%[6] since the first PeLEDs demonstrated in 2014 by Friend et al.[7] Nowadays, the performance of PeLEDs is still under development to pursue that of the advanced organic light-emitting diodes (OLEDs) and quantum dot light-emitting diodes (QLEDs) with the record EQE values exceeding 31% and 27%, respectively.[8]

The dramatic performance improvement of PeSCs and PeLEDs is primarily realized by compositional engineering, morphology modulations, transporting materials designs, interfacial modifications, and defects passivating.[9] These approaches ameliorate the operational stability of PeSCs and PeLEDs simultaneously. PeSCs with a lifetime over 1000 h (T_{80}) have been achieved by several groups,[10] however, such operational stability still cannot meet the 25-year warranty requirement for reliable marketable products.[11] As for PeLEDs, the extremely poor stability with T_{50} lifetime of minutes to hours that demonstrated in laboratories makes such technology far behind commercialization.[12] In order to further improve the performance and retard the degradation of perovskite

optoelectronic devices, we should re-inspect and re-consider the perovskites themselves. As depicted in Figure 1A–D, tuning the precursor ratios and synthesis conditions allows the transformation of halide perovskite structures from bulks (3D), sheets (2D), rods (1D) to dots (0D). The structure of perovskites can be defined at both materials level and morphology level.[13] At materials level, the $[BX_6]^{4-}$ octahedra is isolated by organic molecules to form basic perovskite blocks with dimensions in one or several molecular units for disparate structures from 3D to 0D. The structure variation of halide perovskites at materials level is generally termed as dimensional modulation.[14] At morphology level, the structure variation of perovskite compounds includes bulk, nanoplates/nanosheets, nanorods/nanowires, and nanocrystals/quantum dots. For the low-dimensional perovskites in terms of morphology, they are the 3D networks of $[BX_6]^{4-}$ octahedra in nature and the physical properties of bulk perovskite films are determined by the combination of the type of 3D perovskite unit cell and morphology.

Considering the merits and demerits of halide perovskites with different structures, the assembling of perovskites (named as structural assembling) allows to realize more efficient and stable PeSCs and PeLEDs. The structural assembling strategy is realized in two ways: superposition of more than two types of perovskites or introduction of the additional perovskites into a perovskite host. Through the structural assembling strategy, the merits of different types of perovskites can be
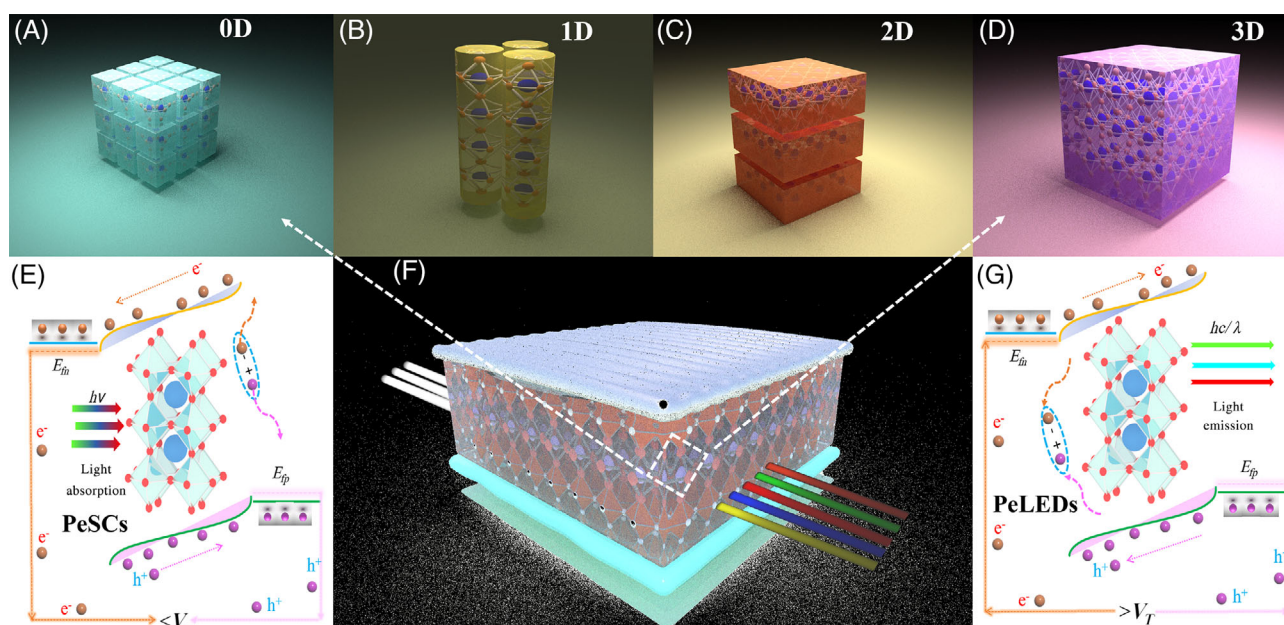

FIGURE 1 Illustration of perovskites with different structures: (A) 0D (nanocrystals), (B) 1D (nanorods), (C) 2D (layer), and (D) 3D (bulk). (E) Schematic illustrations of light absorption and charge carrier extraction processes in PeSCs. (F) A sandwich device structure for both PeSCs and PeLEDs. (G) Schematic illustrations of charge carrier injection and light emission processes in PeLEDs

maximized. For example, an ultra-thin 2D or quasi-2D perovskite layer can help to improve the stability of 3D perovskites,[15] and the 1D perovskites can facilitate the interfacial charge carrier transfer at the 1D/3D perovskite interface.[16] In this review, we first demonstrate the reciprocal working mechanisms of PeSCs and PeLEDs and the factors influencing their optoelectronic performance. According to the working principles of PeSCs and PeLEDs, we then discuss the physical properties of perovskite materials with different structures correlated with the above-mentioned factors. The perovskite layers synthesized with the use of the structural assembling concept and their appealing optoelectronic properties and device performance are then reviewed. Finally, we discuss the potential challenges and present our outlooks on the development of structurally modulated and assembled perovskites for high-performance optoelectronic devices.

2 | RECIPROCITY THEOREMS BETWEEN SOLAR CELLS AND LEDS AND PERFORMANCE DETERMINED FACTORS

The architectures of PeSCs and PeLEDs are similar, comprising a perovskite layer sandwiched by an electron transporting/injection layer (ETL) or a hole transporting layer/injection (HTL),[17] as depicted in Figure 1F. Their working principles are linked by the reciprocity relations.[18] Once in contact with a ETL and HTL, the energy band of the perovskite layer will be bended to align with the Fermi level of the charge transporting layers, which determines the charge carrier extraction and injection of the PeSCs and PeLEDs, respectively. With the development of perovskite-based optoelectronic devices, both organic- and inorganic-based charge transporting materials such as PEDOT: PSS, PTAA, Poly-TPD, Spiro-OMeTAD, CuI, CuSCN, and carbon-based materials for hole transporting, while TiO_2, SnO_2, ZnO, fullerene and its derivatives for the electron transporting have been well-developed for perovskite-based optoelectronic devices.[19] Previous studies have clearly demonstrated that the energy levels, mobilities, and molecular structure of the charge transporting materials are important factors to affect the device performance. Readers have an interest in such topic are recommended to refer to other review articles.[19a,20]

In PeSCs, free charge carriers would be generated in the perovskite layer upon illumination. The electrons and holes would transport toward the selective transporting layer and electrode respectively, to generate electricity (Figure 1E). Reversely, in PeLEDs, electrons, and holes

would be injected into the perovskite layer to recombine and emit photons (Figure 1G). Currently, many theorems have been elaborated to describe the physical processes in PeSCs and PeLEDs, respectively.[21] Considering the complementary physical actions, one could intuitively expect a certain reciprocity theorem to connect device physics of both PeSCs and PeLEDs. The PCE of a solar cell is expressed in Equation (1),

$$PCE = J_{SC} \times V_{OC} \times FF, \tag{1}$$

where J_{SC}, V_{OC}, and FF are short circuit current density, open circuit voltage, and fill factor, respectively. The J_{SC} is determined by suggests the charge carrier generation and collection. V_{OC} is derived from the quasi-fermi level splitting of electrons and holes, and FF is the ratio of the maximum power from the solar cell to the product of V_{OC} and J_{SC}.[17] In thermal equilibrium, the radiative limit for a solar cell is determined by the short circuit current and thermal-equilibrium current (J_{em}) as shown in Equation (2),[22]

$$V_{OC}^{rad} = \frac{kT}{q} \ln\left(\frac{J_{SC}}{J_{em}}\right). \tag{2}$$

However, the practical open circuit voltage V_{OC} equals to V_{OC}^{rad} only if the nonradiative recombination current (J_{nrc}) equals to zero. Under such case, the external quantum efficiency in LEDs is unity based on Equation (3),

$$EQE_{LED} = \frac{J_{em}}{J_{em} + J_{nrc}} = \frac{J_{em}}{J_{inj}}. \tag{3}$$

Here, the J_{inj} is the sum of J_{nrc} and J_{em}, which denotes the current injected in the dark by the applied voltage. Normally, the EQE_{LED} is lower than 1 in the presence of nonradiative recombination due to $J_{nrc} > 0$. According to the diode law,[1b]

$$J_{em} = J_{em,0}\left[\exp\left(\frac{qV}{kT}\right) - 1\right] \approx J_{em,0}\left[\exp\left(\frac{qV}{kT}\right)\right] \tag{4}$$

under the open circuit condition ($V = V_{OC}$), combining the logarithm of Equation (3) into Equation (4), we can obtain the Equation (5) in the following.

$$\ln(EQE_{LED}) = \ln\left(\frac{J_{em,0}\exp\left(\frac{qV_{OC}}{kT}\right)}{J_{inj}(V_{OC})}\right)$$
$$= \frac{qV_{oc}}{kT} + \ln\left(\frac{J_{em,0}}{J_{inj}(V_{OC})}\right). \tag{5}$$

As for a solar cell, the total current amounts to zero, that is, $J_{inj}(V_{OC}) = J_{SC}$ when the device is set at open circuit

condition, and we can obtain the reciprocity theorem (Equation (6)) based on Equations (2) and (5) as

$$V_{OC} = V_{OC}^{rad} + \frac{kT}{q} \ln [EQE_{LED}]. \quad (6)$$

The reciprocity theorem corelates the V_{OC} for a solar cell and the spectral electroluminescence (EL) emission for that photovoltaic device operating as a LED.[22] The current efficiency (CE) of a working PeLED is related to the EL intensity due to the recombination of the injected charge carriers. In order to achieve high EL, the PeLED device should satisfy the following several conditions: (1) A balanced charge injection to maintain the net ratio of electrons and holes in a diode. (2) The injected charge carriers recombine in a radiative pathway rather than a nonradiative process. (3) The generated photons should be efficiently emitted with a high outcoupling efficiency. The three steps can be summarized using an equation as:

$$EQE_{LED} = \eta_{balance} \times PLQY \times f_{outcoupling}. \quad (7)$$

Combining the Equations (6) and (7), the reciprocity theorem is re-demonstrated as:

$$V_{OC} = V_{OC}^{rad} + \frac{kT}{q} \ln \left[\eta_{balance} \times PLQY \times f_{outcoupling} \right] \quad (8)$$

Based on the reciprocity theorem demonstrated above, it is concluded that the excitation and generation of charge carriers and their transfer behaviors greatly influence the performance of PeSCs and PeLEDs.

3 | STRUCTURALLY MODULATED PEROVSKITE FOR PESCS AND PELEDS

3.1 | Structural evolution of perovskites and optoelectronic properties

The solution-processed halide perovskite materials provide great potential for tuning their composition and structure to derive a large number of family members. Various mechanical, physical, and chemical methods have been explored to tailor perovskite structures from 3D to 2D, 1D, and 0D.[13] The term of structural evolution generally leads to a few confusions due to its versatile implications in different situations, in particular for low-dimensional perovskites. As demonstrated in the introduction section, metal halide perovskites have different structures, such as layers (2D), wires (1D), and polyhedrons (0D) at materials level as well as nanoplates/nanosheets (2D), nanorods/nanowires (1D), and nanocrystals/quantum dots (0D) at morphology level. Solution process via spin-coating the chemical solution of organic halide salts and metal halide salts with different stoichiometric ratio are widely used to form perovskite films. As for the modulation of perovskite dimensionality and morphology, various techniques have been used. For example, Lan et al. used chemical vapor deposition (CVD) method to obtain 2D MAPbI$_3$ nanosheets with different thickness for photodetector applications.[23] A combined solution and vapor-phase synthesis method was also reported to achieve 2D perovskites where 2D PbI$_2$ nanosheets were first formed by solution process and then reacted with MAI vapor.[24] The well-known tape exfoliation method was also reported to produce a few layers of (C$_6$H$_9$C$_2$H$_4$NH$_3$)$_2$PbI$_4$ thin flakes from perovskite bulk crystals due to the weak van der Waals interaction between the neighboring 2D perovskite layers.[25] Similar to the 2D perovskite formation, vapor-phase synthesis method was also applicable to form 1D perovskites by growing the lead halide (PbX$_2$) nanowire via CVD deposition first and then reacting with methylammonium halide (MAX) gas.[26] The colloidal synthesis approaches including the ligand-assisted precipitation and hot-injection method are widely reported to synthesize perovskite quantum dots (PeQDs). The ligand-assisted precipitation is realized through reacting the MAX (FAX or CsX) and a long-chain alkyl ammonium halide with PbX$_2$ in the mixed solvents of oleic acid and octadecene. The PeQDs are then precipitated via the addition of acetone and the followed centrifugation.[27] The hot-injection method for PeQDs is normally conducted via the injection of MA-/FA-/Cs-based oleate into a mixed solution of PbX$_2$, oleic acid, and oleylamine in a high boiling solvent (octadecene) at a high temperature.[28] To characterize the perovskites with different structures, scanning electron microscopy (SEM) is a straightforward technique to show the morphologies. X-ray diffraction (XRD) is a powerful analysis to demonstrate the lattice structure of perovskites and the low-angle diffraction peaks are evidence for the formation of low-dimensional perovskite phases.[29] In addition, due to the strong quantum confinement effect in low-dimensional perovskites, spectroscopy methods such as absorption and photoluminescence PL spectra are used to characterize the low-dimensional perovskite.[30] Readers are advised to refer to a previous review paper in *InfoMat* on the synthesis and characterizations of low-dimensional metal halide perovskites.[13] In this work, we will focus on the application of perovskite materials with variable structures for both solar cells and LEDs. Therefore, the structural evolution and assembling are demonstrated in terms of the status of generally used perovskite films, including perovskite materials with dimensions of 3D, 2D, 1D at materials

level, the 0D PeQDs at morphology level, and their combinations.

At materials level, the physical properties of perovskite materials are largely influenced by their dimensional evolution. The unit cell of 3D perovskites adopts a typical cubic structure with a centered corner-sharing $[BX_6]^{4-}$ octahedra. A cation fits in the voids of the octahedra unit to assemble 3D perovskite lattice with a chemical formula of ABX_3. The voids space limits the radius of A cations less than 2.6 Å to form structurally stable 3D perovskite lattice, as determined by Goldschmidt tolerance factor and octahedral factor.[31] Therefore, only a few cations are able to fit for the voids, such as MA^+: methylammonium ($CH_3NH_3^+$), FA^+: formamidinium ($CH_5N_2^+$), and Cs^+. The 3D perovskite exhibits appealing optoelectronic properties, including panchromatic absorption with high absorption coefficients, transient generation of free carriers due to the small exciton binding energy of several meV, defect tolerance ability, and long carrier diffusion length.[14b] The 2D perovskites with the chemical formula of A_2BX_4 have a layered structure that is cut from a 3D perovskite along a specific direction to form a segment of the corner-sharing $[BX_6]^{4-}$ octahedra layer separated by long/large organic chains.[32]

Compared with 3D perovskites, layered 2D perovskites have less restrictions on cation sizes, enabling wide choices on the selection of organic cations for versatile 2D perovskites formation. The organic layer has a relatively large HOMO-LUMO energy gap and a large dielectric mismatch with the inorganic layer, rendering multilayer quantum wells structure for 2D perovskites. The quantum-confined 2D perovskites exhibit disparate optoelectronic features from 3D perovskites.[14b] The electric field generated by charges in the inorganic quantum well framework (high dielectric constant) extends into organic barriers with low dielectric constant, reducing the dielectric screening of organic layers. As a result, the reduced dielectric screening effect enhances binding energies of 2D perovskites up to several hundred meV to form stable excitons.[33] We describe the dielectric confinement difference between 2D perovskites and 3D perovskites in Figure 2A. The strong excitonic behavior due to the dielectric confinement effect contributes to a strong PL peak and a high photoluminescence quantum yield (PLQY) for 2D perovskites. In addition, the bandgap of 2D perovskites is generally higher than 3D perovskites, leading to a narrower light absorption range.[37]
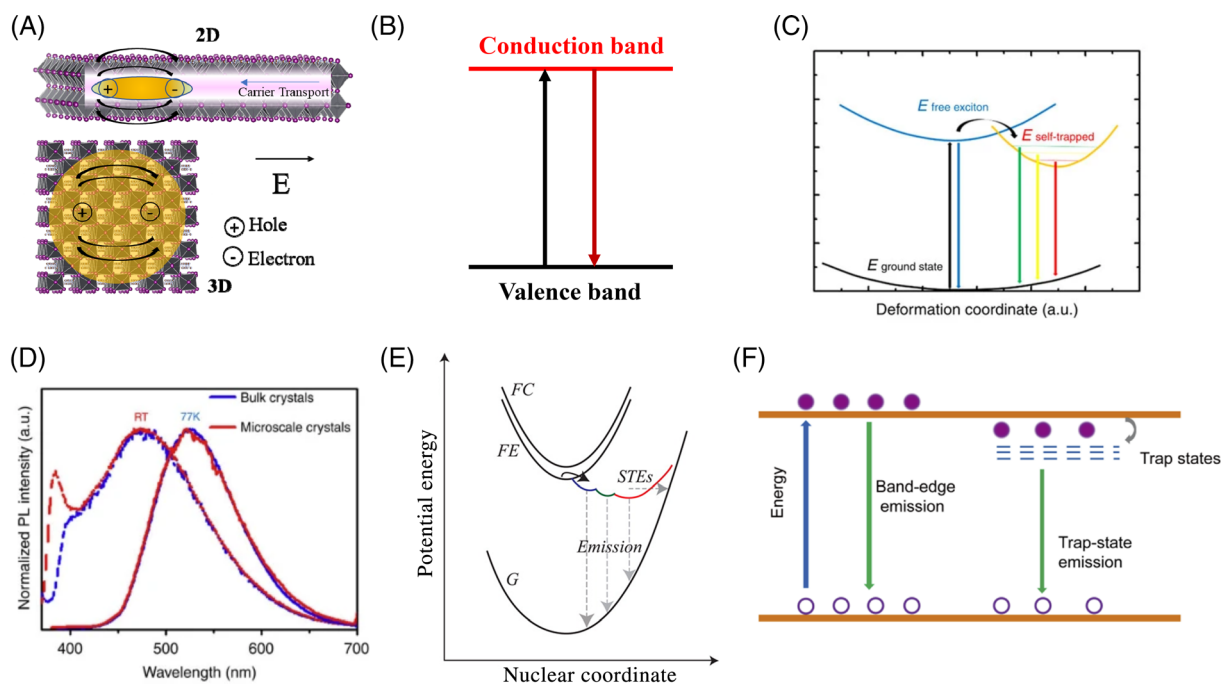

FIGURE 2 (A) Schematic illustrations of dielectric confinement in 2D perovskites versus 3D perovskites. (B) Direct band emission mechanism for 3D perovskites. (C) Mechanism for emission from both direct band and self-trapped states in 2D and 1D perovskites. (D) Emissions of the bulk and microscale 1D perovskite crystals (excited at 360 nm) at room temperature (dash lines) and 77 K (solid lines). (C) and (D) Reproduced under the terms of the Creative Commons CC BY license from Reference 34. Copyright 2017, Springer Nature. (E) Mechanism for emission from a reorganized excited state in 0D perovskites. Reproduced with permission from Reference 35. Copyright 2016, American Chemical Society. (F) Various excited-state decay pathways for $CsPbBr_3$ QDs. Reproduced with permission from Reference 36. Copyright 2020, American Chemical Society

The 1D perovskite wire is structurally connected by the metal halide octahedra via corner-sharing, edge-sharing, or face-sharing configurations and organic cations surround the inorganic octahedra outside. Depending on the connect manner among octahedrons, the configurations of 1D perovskites could be either zigzag or linear with variable chemical formulas. Only one degree of freedom does exist in 1D perovskites. The high level of spatial confinement in two directions thus enlarges the binding energy to several hundred levels, resulting in the stronger quantum confinement for an increased PLQY.[38] In addition, the spatial confinement of 1D perovskites will prompt carrier transfer in a given direction but constrains charge transport capabilities in other directions.

0D perovskite polyhedrons have a structure of the individual metal halide octahedra surrounded by organic cations. The 0D perovskites molecular units are connected periodically to form bulk materials with the general chemical formula of A_4BX_6. In contrast to the 0D perovskite polyhedrons, the 0D PeQDs are formed through surrounding either a 3D perovskite cluster or 2D perovskite cluster with long-chain ligands to a size of several or several tens of nanometers. Although the structure of 0D perovskite polyhedrons and 0D PeQDs are different, they have the spatial confinement effect in common. The 0D perovskites have zero degree of freedom with a dimension smaller than the exciton Bohr radius. The measured ultra-large exciton binding energy ranging from 84 to 320 meV in 0D perovskites reduces the exciton dissociation probability to show the enhanced light emission.[39]

3.2 | Excited-state physics and PL emission in perovskites

Based on the discussion above, one of the core discrepancies among perovskite materials with various structures is the exciton binding energy. With the reduction of dimensionalities from 3D to 0D, the exciton binding energy of perovskites increases from a few meV to hundreds of meV. The exciton binding energy directly determines the excited-state physics and excitons behaviors of perovskites with different dimensionalities. As for the 3D perovskites, there are strong interactions between metal halide octahedra, resulting in the formation of delocalized excitonic band characteristic. As shown in Figure 2B, upon excitation, the charge carriers are directly excited from the valence band to the conduction band in a band-to-band approach.[30] As a result, the PL emission of 3D perovskites generally has a small Stoke shift with a narrow full width at half maximum (FWHM).[21c] With the reduction of dimensionalities, the excitonic effects would be strengthened due to the increased exciton binding energy. The enhanced excitonic effect results in a strong electron–phonon coupling. In a lattice distortion field with the presence of a strong exciton-lattice coupling, the bound excitons would be self-trapped as a small polaron. Such phenomenon is called "self-trapped exciton" (STE). As for 2D and 1D perovskites, electrons, after being excited to free-exciton excited states, would relax to STE with multiple trapped states promptly (Figure 2C). As a result, self-trapping of excitons in 2D and 1D perovskites lead to broad-bands, Gaussian-shaped, and strongly Stoke-shifted luminescence (Figure 2D).[34] As depicted in Figure 2E, the STE is easy to form in 0D perovskite polyhedrons because there is no potential energy barrier between the excited electrons and STE.[35] Upon excitation, high energy excited states would induce ultrafast structural reorganization of excited states to release toward lower-energy excited states so that strongly Stokes-shifted broad-band emissions with high PLQY values can be obtained.[40]

As for PeQDs, the weak electron–phonon coupling under ambient conditions determines the relatively small STE binding energy.[41] Excited electrons are more easily to transit from valence band to conduction band and bound excitons are readily to form due to strong quantum confinement owing to the unique structure of PeQDs. The formed bound excitons will contribute to a band-edge emission with narrow FWHM and high PLQY. However, the undercoordinated surface atoms with dangling bonds often occur when the surface ligands are removed during the film formation. Then the undercoordinated surface atoms would act as localized trap states for carriers and thus quench the PL emission, as shown in Figure 2F.[36]

3.3 | Charge carrier recombination and transport in perovskites

The carrier transfer dynamics which determine the performance of perovskite optoelectronic devices is found to be correlated with the structure of perovskites.[42] Generally, recombination pathway plays significant roles in carrier transfer processes for all types of perovskite-based optoelectronic devices. The carrier recombination processes include radiative and non-radiative recombination. The non-radiative recombination occurs via deep defect states in the band and is responsible for the energy offset between the charge transfer (CT) state and the V_{OC} state (see Figure 3A). The recombination dynamics depend on carrier densities in the active layer under different excitation levels. As shown in Figure 3B, geminate recombination (monomolecular) dominates the carrier decay when the free carrier density n_0 falls in the range of 10^{13}–10^{15} cm^{-3} under low excitation. In contrast, nongeminate recombination (bimolecular) and
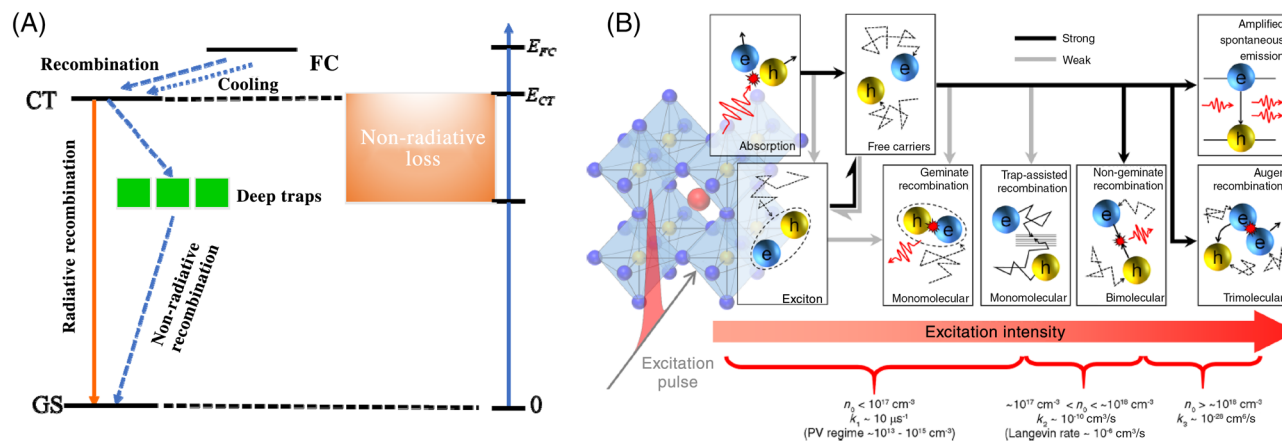
FIGURE 3 (A) Schematic illustration of the carrier recombination process. GS: ground state; CT: charge transfer state; FC: free carriers. (B) Various photophysical processes and recombination rates in perovskite materials over a range of photoexcited carrier densities, n_0. Reproduced with permission from Reference 43. Copyright 2016, American Chemical Society

Auger recombination (trimolecular) become dominant in the regime of high carrier densities of 10^{16}–10^{18} cm^{-3}.[43] The whole recombination process is depicted by the following equation:

$$\frac{dn}{dt} = -k_1 n_0 - k_2 n_0{}^2 - k_3 n_0{}^3, \tag{9}$$

where k_1, k_2, and k_3 are the first-order process, the second-order process, and the third-order process rate constants corresponding to the monomolecular recombination, bimolecular nongeminate recombination, and Auger recombination, respectively. The Auger recombination and the monomolecular recombination include the intrinsic defect-assisted recombination and the band-tail indirect recombination, contributing to the non-radiative recombination losses. Theoretical calculation has proved that the photocarrier density in typical PeSCs falls in the range of 10^{14}–10^{15} cm^{-3} under AM 1.5G illumination, which is suited in the first-order recombination regime.[44] Therefore, the monomolecular recombination is considered to be a major photocarrier loss in PeSCs.

These recombination pathways also apply to PeLEDs and influence the carrier-densities dependent internal luminescent yields in the perovskite emitter. In PeLEDs, electrically injected excited carrier densities in the range of 10^{15}–10^{17} cm^{-3} will produce a high internal luminescence yield (>90%).[21c,45] In contrast, with a lower carrier density (<10^{14} cm^{-3}), the luminescence yield is extremely low (<1%) unless the non-radiative recombination could be significantly suppressed. On the other hand, the Auger recombination becomes the main killer of luminescence yield when the carrier density is higher than 10^{17} cm^{-3}. Together with carrier density effect, the mobility of transporting materials[9c,17] and interfacial defects[1b,9b] are also found to influence the carrier diffusion length and lifetime of perovskite films.

As shown in Figure 4A, in 3D perovskites, the photo-generated free carriers would relax from high-energy excited states to low-energy ground states (GS) spontaneously with different time scale for different processes.[46] The carriers are inevitably thermalized because the short-wavelength light possesses energy greater than the bandgap of perovskites to pump carriers to energy positions higher than the conduction band minimum (CBM). After thermalization, hot carriers begin to cool down to the charge transfer states (CT) accompanied by the release of thermal energy.[49] As reported by Beard et al., the cooling time of hot carriers could be ultralong up to 100 ps,[50] and such long relaxation process of hot carriers provides an opportunity to further lift the efficiency of PeSCs to overcome the Shockley-Queisser limit. After cooling down, the carriers have to undergo the next transport processes within several nanosecond to microsecond, where a dynamic competition exists between the recombination and the extraction. As for 3D perovskites, a peculiar property is the slight Stokes shift for PL emission and exceptionally sharp absorption onset over 10^4 cm^{-1} above the absorption edge. Due to the high radiative recombination rates and the long carrier lifetimes, the Stokes shift of perovskites induces the simultaneous occurrence of absorption and reemission of excited carriers, leading to the photon recycling in 3D perovskite films.[21c] This multiple absorption-diffusion-emission process has been experimentally verified via the observation of the photocurrent detected at over 50 μm away from the photoexcited position in a lateral-contact architecture solar cell (Figure 4B).[47] Apart from the 3D perovskite, the photon recycling is also observed in quasi-2D perovskite materials.[51] The existence of the photon recycling in perovskite materials can enhance the externally outcoupled PL of perovskites and thus improve the voltage characteristic of PeSCs.[45] Likewise, owing to the high luminescence efficiency of perovskite materials, the photon recycling could facilitate the light
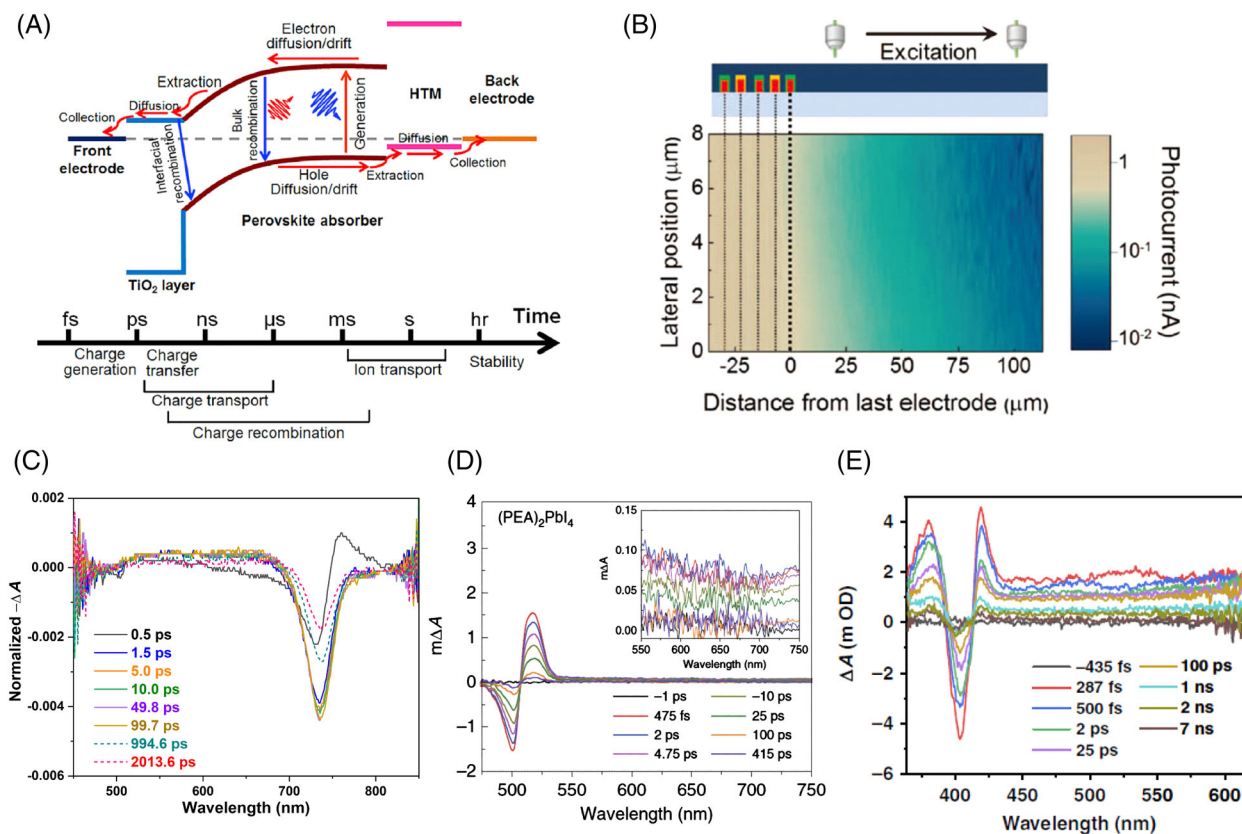
FIGURE 4 (A) Charge carrier processes and the corresponding timescale in 3D perovskite optoelectronic devices. Reproduced with permission from Reference 46. Copyright 2018, Elsevier. (B) Photocurrent map at the edge of the active area of an interdigitated back-contact perovskite-based device. The lateral position is along the electrode direction. The photocurrent is observed at sites several tens of micrometers beyond the last electrode (x-axis position 0 mm, bold dashed line). Reproduced with permission from Reference 47. Copyright 2016, The American Association for the Advancement of Science. TA spectra of (C) 3D CsFAMA perovskite, Reproduced with permission from Reference 48a. Copyright 2020, John Wiley and Sons. (D) 2D PEA_2PbI_4 perovskite, Reproduced under the terms of the Creative Commons CC BY license from Reference 48b. Copyright 2018, Springer Nature, and (E) 0D $(C_3H_{11}N_3O)_2PbBr_6$ perovskite. Reproduced under the terms of the Creative Commons CC BY license from Reference 48c. Copyright 2019, Springer Nature

outcoupling via randomizing propagation directions of photons and redirecting the photons outcoupling from trapped states.[21c,51] Therefore, different from other types of LEDs that re-absorption of the emitted light is a typical light loss, the photon recycling phenomenon would benefit the enhancement of outcoupling efficiency of 3D PeLEDs.

With the reduction of dimensionalities of perovskite materials, the excitation, and relaxation span decreases owing to the increased exciton binding energy. Figure 4C–E show the transient absorption (TA) spectra of a mixed-phase 3D perovskite, a 2D PEA_2PbI_4 perovskite and a 0D $(C_3H_{11}N_3O)_2PbBr_6$ perovskite.[48] For all samples, there are detectable photobleaching (PB) signals located at the band edge region. Free carriers are formed spontaneously within 1 ps for 3D perovskites. After generation, the excited carriers would relax via two pathways (Figure 4C), including a several hundred ps pump-fluence dependent lifetime induced by the bimolecular recombination and a several thousand ps lifetime derived from trap-assisted monomolecular

recombination.[48a] Compared with 3D perovskites, a shorter lifetime is observed for 2D perovskites, such as approximately 100 ps GS bleaching recovery shown in Figure 4D.[48b] 1D perovskites have a similar exciton recombination lifespan to the 0D perovskite.[48c] Take the 0D $(C_3H_{11}N_3O)_2PbBr_6$ perovskite crystal as an instance. Upon photoexcitation, the as-formed excitons relax to multiple states within different energies caused by the STE phenomenon within several ps (Figure 4E).[48c] In addition, low dimensional perovskites show a larger Stokes shift effect, indicating that the photon cycling phenomenon become less important than that in 3D perovskites.

As for PeQDs, multi-excitonic states (MESs) were observed during the excitation process. It is found that MESs is produced by direct multi-exciton generation, that is, the absorption of a single photon with sufficiently high energy generates more than one exciton. The MESs account for the high PLQY values in PeQDs. During the relaxation, the first electron transfers in a rapid speed. After that, the driving force for the next electron

transfer become smaller due to the increased Coulomb potential and the lower energy of the next available exciton. Such multi-exciton transfer process has been observed in PeQDs previously.[52] As estimated, the electron transfer of the multi-excitonic state could be as short as within 1 ps.[53] Although the multi-excitonic behaviors is favorable to obtain a high PL emission in PeQDs, the Auger recombination would play a more essential role in nonradiative process under multiexciton generating regime.

3.4 | Formation energy and stability of perovskites

The stability of perovskite materials is strongly affected by their lattice structure. As shown in Figure 5, the formation energy of perovskites with different structures is calculated by density functional theory approach.[54] The 0D perovskite polyhedrons have the lowest formation energy of −0.69 eV in perovskite family, indicating their intrinsic unstable characteristics. Compared to the widely used 3D perovskites with the formation energy in a range of −0.95 to −0.85 eV, both 2D and 1D perovskites show an increased formation energy in the range of −2.68 to −1.51 eV and −2.27 to −0.99 eV, respectively. Therefore, 2D and 1D perovskites are more thermodynamically stable than 3D perovskites, providing an approach to improve the stability of 3D perovskites optoelectronic devices through perovskite dimension management. In addition to the higher formation energy of 1D and 2D perovskites, bulky ammonium cations used in 2D perovskites are generally hydrophobic, strengthening the film resistivity to humid environment.[14a,37] In 1D perovskites, the $[MX_6]^{4-}$ octahedra are connected shoulder to shoulder, which promotes the skeleton strength of perovskite lattices. Furthermore, the $[MX_6]^{4-}$ octahedra in 1D perovskite lattice is wrapped by inactive organic cations to avoid the direct exposure to moisture and oxygen.[55] As for PeQDs, surface ligands have risks to secede from the surface of PeQDs and undergo a fast exchange between free states and bound states. The unstable surface of PeQDs causes the aggregation of adjacent PeQDs, leading to severe challenges for their deployments.[56] The unique physical properties and phase stabilities of perovskites with different structures render them different advantages in the applications of PeSCs and PeLEDs, which is briefly reviewed and summarized in the following section.

4 | AN OVERVIEW OF PESCS AND PELEDS BASED ON SINGLE STRUCTURE PEROVSKITES

In Section 2, we analyzed the reciprocity theorems between solar cells and LEDs and factors determining the device performance. These factors are related to the specific structures of metallic halide perovskites. Therefore, the structural evolution of perovskites and their impact on the optoelectronic properties are discussed in Section 3, including excited-state physics, PL emission, charge carrier transport and recombination, formation energy, and phase stability. Based on these discussions, the developments of solar cells and LEDs using different structural perovskites are elaborated in this Section 4. Then the development of PeSCs and PeLEDs based on perovskite structure assembling engineering will be further overviewed in Section 5.

4.1 | 3D perovskites for PeSCs and PeLEDs

3D perovskites are widely used for developing highly efficient PeSCs because free charge carriers are generated in perovskite layer upon light illumination. Alongside the deeper understanding of 3D perovskites, various effective
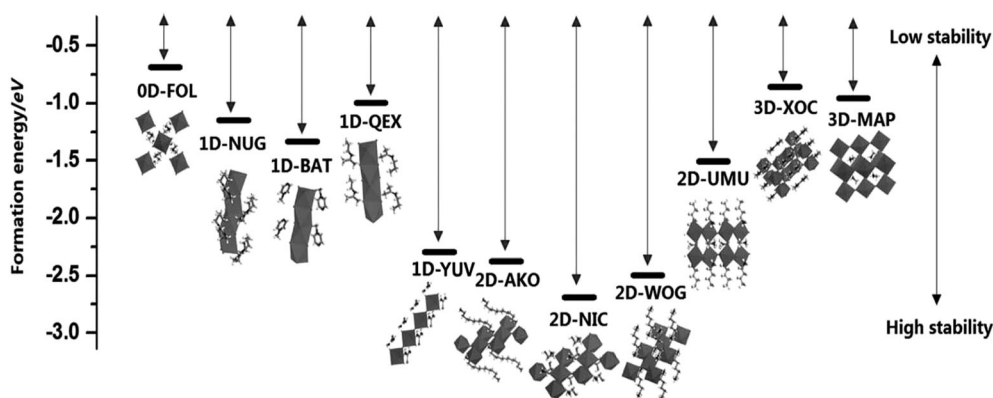

FIGURE 5 The formation energies of 0D-FOL, 1D-NUG, 1D-BAT, 1D-QEX, 1D-YUV, 2D-AKO, 2D-NIC, 2D-WOG, 2D-UMU, 3D-XOC, and 3D-MAP. Reproduced with permission from Reference 54. Copyright 2017, The Royal Society of Chemistry

approaches have been illustrated to improve the efficiency to 25.5%. Meanwhile, the stability of PeSCs have been enhanced to maintain more than 90% of their initial efficiency for 1000 h testing under moisture, thermal stress, and light illumination through precisely passivating defects, suppressing ion migration, etc.[57]

The relatively small exciton binding energy limits the luminance efficiency for efficient PeLEDs. Two effective strategies have been exploited to enhance the luminance efficiency of PeLEDs: (1) spatial confinement of charge carriers to lift the excitonic recombination rate, and (2) defects passivation to reduce the defect-induced non-radiative recombination. A breakthrough was achieved in green PeLEDs with a high EQE of 20.3% and a strong luminance of 14 000 cd/m^2 by Wei and cooperators.[58] They took advantage of the different solubility and crystallinity behavior between the $CsPbBr_3$ perovskite and MABr passivated agent in polar solvents to produce sequential crystallization of $CsPbBr_3$ perovskite coated with MABr. This sequential crystallization process finally yielded a $CsPbBr_3$/MABr quasi-core/shell structure, which provided a place for light-emitting. In addition, the MABr shell passivated defects in grain boundaries simultaneously balanced charge injection, thus yielding a high PLQY of 80%. A near infrared PeLED with an EQE of 20.7% was reported through introducing amino-acid additives into the perovskite precursor solution. The introduced amino-acid additives controlled the growth of the $FAPbI_3$ perovskite to spontaneously form submicrometer-scale structures with reduced surface defects.[59] In another work, Xu et al. pointed out that the amino group in the reported passivation molecules was insufficient because it could form stronger hydrogen bonds with the organic cations in perovskites and thus attenuate its passivation effect.[60] Both hydrogen bonds and passivating coordination bonds are stemmed from the long pair electrons at nitrogen atoms in amino groups. The oxygen (O) atoms were capable to polarize amino groups to reduce the hydrogen bonding ability. A rational design of passivation molecules was illustrated by modulating the position of O atoms to strengthen the interaction between the passivation agents and perovskite defects to record the highest EQE of 21.6% for the near-infrared PeLEDs based on the $FAPbI_3$ perovskite. Benefited from the extremely efficient defects passivation, the half-lifetime of PeLEDs is improved from 1.5 to 20 h at a constant current density of 25 mA cm^{-2}.

4.2 | 2D perovskites for PeSCs and PeLEDs

In contrast to 3D perovskites, one of the unique features of 2D perovskites is the facile structure tunability through the molecular design of organic cations for different chemical and optoelectronic properties. Various types of organic cations were investigated to synthesize new 2D layered perovskites, as summarized in a previous review article.[61] 2-phenylethylammonium (PEA) and n-butylammonium (n-BA) are the most widely used organic cations to synthesize 2D perovskites consisting of single $[PbX_6]^{4-}$ octahedra sheets separated by bilayers of organo-ammonium cations with the general formula of $(PEA)_2PbX_4$ or $(BA)_2PbX_4$.[62] The Two-photon absorption (TPA) properties with a giant TPA coefficient which is one order of magnitude higher than 3D perovskites were observed in 2D $(PEA)_2PbI_4$ perovskites. Moreover, the TPA coefficient was negatively correlated with the thickness, indicating unique optical properties of 2D perovskites.[63] A systematic theoretical calculation was performed to further understand the unique properties of 2D perovskites. It was found that the carrier mobilities of 2D perovskites are much smaller than that of 3D perovskites, whereas the exciton binding energy is greatly enlarged. Moreover, the 2D $(PEA)_2PbI_4$ perovskite exhibits a strong linear dichroism, indicating extremely weak absorption along the c axis in the visible spectrum.[64] Despite of the enlarged exciton binding energy, the luminescence of the 2D perovskite can only be conditionally observed at low liquid-nitrogen temperatures due to the thermal quenching of excitons.[65] Moreover, the insulating of the bulky organo-ammonium cations impede efficient charge transport and thus constrain the luminescence efficiency of 2D perovskites.[66] All these physical properties investigation indicates that 2D perovskites are unsuitable to be used as photovoltaic or light-emitting materials. The 2D perovskites are generally integrated with 3D perovskites in the form of quasi-2D perovskites or 2D/3D mixed perovskites to modulate carrier dynamics and phase stability for the applications of PeSCs and PeLEDs, which will be discussed in the following section of structural assembling perovskite. The strong spin-orbit coupling (SOC) was observed in the 2D perovskite, which split the spin-degenerate bands in its non-centrosymmetric structure, thus generating the Rashba splitting.[67] The Rashba splitting observed in non-centrosymmetric 2D perovskites is indicative of promising nonlinear photodetection. Experimentally, excellent light responsivities were observed based on the 2D $(PEA)_2PbI_4$ single crystalline perovskite with anisotropic optoelectronic properties.[68]

4.3 | 1D perovskite for PeSCs and PeLEDs

1D perovskites present superior anisotropic optical and electrical properties. The anisotropic optoelectronic

properties of 1D perovskites contribute to the better conductivity of charge carriers in a specific direction and the higher photoluminescence due to the spatial quantum confinement.[38] For the device development, a PCE of 14.71% was achieved in PeSCs based on $MAPbI_3$ perovskite nanowires.[69] After this pioneer work, several works[70] controlling the nucleation and the growth of 1D perovskites as well as exploring appropriate transporting materials have been reported to further improve the PCE to 18.83% with a T_{80} of 1500 h.[71] However, the PeSCs based on 1D perovskites finally failed to be dramatically developed and we ascribe its sluggish to the mismatching of the nanowire or nanorod perovskite morphology with the planar or mesoporous solar cell architectures that require full coverage of each layer to guarantee the balanced and efficient interfacial charge transport. The reason of severe interfacial charge recombination also hinders the development of PeLEDs using 1D perovskites as the light emitter, despite their observed high photoluminescence. To the best of our knowledge, only few works have been reported regarding the luminesce phenomenon of 1D perovskites.[34,48c]

4.4 | PeQDs for PeSCs and PeLEDs

PeQDs are universally explored for the applications of PeSCs and PeLEDs due to their optoelectronic properties such as multiexciton generation, additional bandgap tuning via quantum-confinement effect, near-unity PLQY, easily-processable colloidal synthesis compatible for industrial manufacturing.[72] It is found that the α-phase $CsPbI_3$ PeQDs can sustain its cubic phase at low temperature and show size-controlled band gap and long-range electronic transport. The first PeSCs based on the $CsPbI_3$ PeQDs showed a PCE of 10.77% with a high V_{OC} of 1.23 V. Such PeSCs also exhibited bright red electroluminescence under a low turn-on voltage of 1.8 V, indicating its potential for light-emitting applications.[72] Since then, a series of works were committed to promote the performance and stability of PeSCs and PeLEDs based on PeQDs. For solar cells, the electronic coupling between $CsPbI_3$ PeQDs was tuned through a post-treatment by cation halide salts to enhance their carrier mobility and achieved a high PCE of 13.43%.[73] Through using a ligand-assisted cation-exchange strategy, mixed cation $Cs_{1-x}FA_xPbI_3$ PeQDs was synthesized with long carrier lifetime[74] due to the enhanced orbital overlap and the easier polaron formation resulted from the fast rotation of FA.[75] Moreover, the concomitant occupation at A site by FA and Cs decreased the entropic formation energy of the mixed cation PeQDs.[9a] Consequently, a record efficiency of 16.6% was achieved with improved device stability (T_{95}: 600 h).[74]

For LED application based on PeQDs, in 2014, $MAPbBr_3$ PeQDs with a diameter of 6 nm was firstly synthesized using medium-sized chain assisted synthesis method, which emitted green light with a narrow bandwidth and a decent PLQY of 20%.[27] Shortly after, the PLQY was lifted to 70% for $MAPbBr_3$ PeQDs by using a ligand-assisted re-precipitation method[76] and to 93% via temperature controlling the ligand-assisted re-precipitation process.[77] In order to enhance the stability of PeQDs, all-inorganic $CsPbX_3$ based PeQDs was synthesized and showed a high PLQY of 90%.[78] The excellent optical properties of PeQDs imply their great potential in the display technology, but the preliminarily fabricated PeQDs LED exhibited an EQE of 0.12%.[79] Despite the moderate device performance, this groundbreaking work testified the possibility of achieving PeQDs LED and attracted tremendous research interest in the improvement of the device performance and stability via various approaches such as surface engineering, composition engineering, defects passivation, etc.[80] Particularly, Kido et al. achieved the state-of-the-art red PeQDs LED with a striking EQE of 21.3% and a longer T_{50} lifetime of 180 min using an anion exchange method.[81] As for Green PeQDs LED, a breakthrough was reported recently via modulating the organic cation and surface passivation of halide defects to achieve an EQE of 23.4% with a T_{50} of 132 min.[6]

5 | STRUCTURALLY ASSEMBLED PEROVSKITES FOR PESCS AND PELEDS

Perovskite materials with structural modulation have exhibited tunable optoelectronic properties such as optical bandgaps, which is generally due to the organic cations doping and metallic cations doping as summarized in other review articles.[82] For example, doping organic amine cations with long alkyl chains to partially replace the commonly used MA and FA cations will not only reduce the dimension of perovskites, but also modulate the bandgap of the resulting perovskites.[83] It has been demonstrated that long alkyl chains in the low-dimensional perovskites can increase the steric hindrance effect in perovskite lattice, and thus manipulate and stabilize the corresponding structurally assembled perovskites.[84] Therefore, It is foreseeable that the use of more than one perovskite structural building blocks in the perovskite layer (structural assembling engineering) will help to take full advantage of their unique properties for efficient PeSCs and PeLEDs. In this section, we review and discuss the reported works regarding perovskite structure assembling engineering for the applications of both PeSCs and PeLEDs.

5.1 | Quasi-2D perovskites for PeSCs and PeLEDs

Although the 2D perovskites with a monolayer of $[PbX_6]^{4-}$ octahedra are not suitable for solar energy harvesting or luminescence application, combining the 3D perovskite features with 2D perovskites to assemble the quasi-2D Ruddlesden-Popper (RP) perovskites is a hot topic for the applications in PeSCs and PeLEDs. The general formula for the class of quasi-2D perovskites is $(RNH_3)_2A_{n-1}Pb_n X_{3n+1}$, where RNH_3 is the bulky aromatic or aliphatic alkylammonium spacer cation, for example, PEA or BA for 2D perovskites, A is the monovalent organic/alkaline cation, for example, MA, FA, and Cs for 3D perovskites. The thickness of the inorganic sheet could be tuned by the stoichiometric ratio between the small cation and the spacer cation, and in turn, the optoelectronic properties, including the bandgap, the exciton binding energy, and carrier dynamics.[14b,85] Due to the layer thickness-dependent optoelectronic properties, quasi-2D perovskites exhibit strong light absorption in the visible region when $n \geq 3$ for photovoltaic applications, and strong PL at room temperature for the use of LEDs.[86]

5.1.1 | PeSCs

In 2014, the quasi-2D $(PEA)_2(MA)_2Pb_3I_{10}$ perovskite was used as the light absorber for the first time. Despite the low efficiency of 4.73%, the excellent moisture resistance even after storage for 46 days under 52% RH was attracting enough to temporarily address the stability issue of the widely studied 3D PeSCs.[87] At that time, the quasi-2D $(BA)_2 (MA)_2Pb_3I_{10}$ was also applied and exhibited ultralong stability over 2 months under 40% RH, but a low PCE of 4.02%.[85] The low efficiency is ascribed to the growth of the quasi-2D perovskite with a lateral alignment of inorganic layers because the large spacer cations preferentially adapt to the alignment parallel to the substrate. As revealed, the vertically oriented 2D perovskite thin film offers the direct pathway for carrier transport, nevertheless, the carriers have to hop across the long-chain organic surface ligands in the randomly oriented film. The effect of the orientation of quasi-2D perovskites on the charge transport and the photovoltaic performance is schematically illustrated in Figure 6A–E.[88] A hot-cast method was proposed to align the quasi-2D perovskite growth perpendicular to the substrate, thereby dramatically expediating the charge transport across the film.[37] As a result, a PCE of 12.52% was achieved and was further enhanced to 14.3% through using the substrate effect.[91] Despite this breakthrough, the hot cast method generally requires to heat substrates to over 100°C before depositing the precursor solution, which imposes

difficulties of accurately controlling the temperature and the thermal homogeneity of substrates for reproducible PeSCs. This challenge was then alleviated through introducing the 2-thiophenemethylammonium (ThMA+) as the spacer cation coupled with MACl additives to achieve a high PCE of 15.42%.[92] Except for the exploring new spacer cations, it was solved by partially replacing the MA^+ with the BA^+ spacer cation to form the $BA_{1.6}MA_{3.4}Pb_4I_{13}$ quasi-2D perovskite. Such quasi-2D perovskite film possesses highly oriented grains and uniform grain size distribution without the requisite of preheating process and yielded a reproducible 15.44% PCE that could be stored for a long term.[93]

The origin of the significant influence on the charge transport capability by the orientation of quasi-2D perovskites is stemmed from the insulating characteristic of large organic spacer cations. It was found that dominant photocurrent is collected through the electric field-assisted exciton separation and transport across potential barriers built by spacer cations.[94] Two main strategies including the thickness modulation of inorganic sheets and optimizing organic cations have been developed to overcome this obstacle. As depicted in Figure 6F, with increasing the number of the inorganic octahedra sheet (n) between two adjacent organic spacers, PeSCs exhibit enhanced PCE approaching to that of PeSCs based on 3D perovskites ($n = \infty$). However, the formation energy tends to lower to sacrifice the device stability.[89] In order to take full advantage of the outstanding stability of the 2D perovskite, most of the quasi-2D perovskites with $n = 3$ or 4 are selected as the candidate for light absorption.[14] Cs^+ or FA^+ cations have been used to incorporate in quasi-2D $(BA)_2(MA)_2Pb_3I_{10}$ perovskites to control the crystallization kinetics and reduce nonradiative recombination centers so that the PCE was improved to 13.7% and 12.81%, respectively.[95] A recent work further explored the incorporation of dual cations of Cs^+ and FA^+ into quasi-2D perovskites to enhance the charge transport and achieved a high PCE of 14.23%.[96] In addition to the modulation of small cations in quasi-2D perovskites, the combination of the typical PEA^+ and BA^+ to be the spacer cation was exploited to yield efficient quasi-2D PeSCs with a PCE of 15.46%.[97] It was found that the incorporation of PEA^+ in quasi-2D perovskites could offer π electron to interact with I^- of PbI_6^{4-} to decrease the exciton binding energy for efficient charge transfer. In addition to the cation modulations, new spacer cation was explored to yield high-performance quasi-2D PeSCs. For example, 3-bromobenzylammonium iodide (3BBAI) based quasi-2D perovskites were synthesized.[90] The 3BBAI based quasi-2D perovskites exhibited a high degree of electronic order and structure orientation, consisting of ordered large-bandgap perovskites vertically grown in the bottom region and oriented small-bandgap located on the top (Figure 6G), as derived from the GIWAX spectra shown
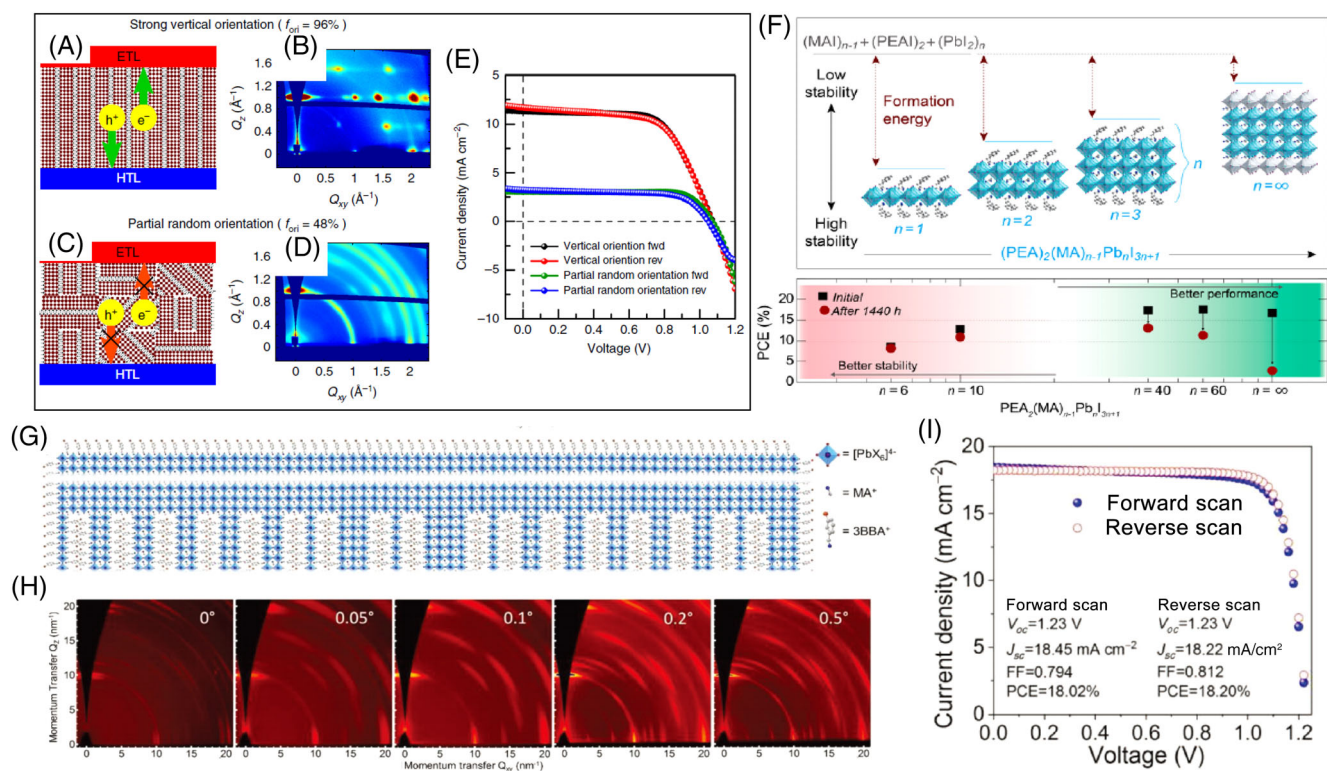
FIGURE 6 Charge transport and device performance with different degrees of orientation. (A) Pre-crystallization annealed film provides direct pathways for electron and hole extraction. (B) GIWAXS results show the film with strong vertical orientation. (C) Post-crystallization annealed film charge carriers need to hop through electrically insulating organic ligands to reach ETL and HTL. (D) GIWAXS results show the film with partial random orientation. The percentage of oriented crystallites in the perovskite film is defined as f_{ori}. (E) The performance of PeSCs fabricated using the pre-crystallization annealing method (red and black lines) is significantly higher than that of the post-crystallization annealing method (green and blue lines). (A)–(E) Reproduced under the terms of the Creative Commons CC BY license from Reference 88. Copyright 2018, Springer Nature. (F) The influence of the thickness of the inorganic sheet number n on the formation energy, efficiency, and stability of quasi-2D PeSCs. Reproduced with permission from Reference 89. Copyright 2016, American Chemical Society. (G) Schematic illustrations of the proposed self-assembled 3BBA-based quasi-2D perovskite film structure. (H) GIWAXS images to show the structure of the quasi-2D perovskite film. The incidence angles are 0°, 0.05°, 0.1°, 0.2°, and 0.5°. (I) J–V curve for the champion cell based on quasi-2D perovskites. (G)–(I) Reproduced with permission from Reference 90. Copyright 2018, John Wiley and Sons

in Figure 6H. The ordered structure suppressed the non-radiative recombination and facilitated the charge transport. Consequently, the highest PCE of 18.20% with the improved V_{OC} and FF (Figure 6I) in quasi-2D PeSCs was recorded.[90] Moreover, such highly efficient quasi-2D PeSCs could be stored for a long duration (retaining 82% of the initial efficiency over 2400 h). Other spacer cations were also widely explored to realize highly efficient quasi-2D PeSCs, as summarized by the previous review discussing the principles for the molecule design of spacer cations.[98]

5.1.2 | PeLEDs

The multi-quantum well structure of quasi-2D perovskites renders them an enlarged binding energy to yield a strong PLQY for efficient PeLEDs. In 2016, Sargent et al. firstly assembled the quasi-2D $PEA_2MA_{n-1}Pb_nI_{3n+1}$ for near-infrared PeLEDs application.[99] After optimizing the stoichiometric ratio between the PEA^+ and the MA^+, an EQE of 8.8% and a radiance of 80 W/sr/m^2 was recorded when n equals to 5. More importantly, the typical funnel-like carrier transport model was demonstrated by analyzing carrier dynamics of quasi-2D perovskites. They found that quasi-2D perovskites exhibited an inhomogeneous energy landscape and charge carriers could funnel from high-bandgap parts to the low-bandgap ones, ultimately concentrating these carriers on the smallest bandgap zone. The energy transfer through the funnel route could complete within 1 ps through passivating nonradiative recombination pathways by using a wide-optical-gap polymer (poy-HEMA).[100] The quasi-2D perovskite-polymer heterostructure film displayed an ultra-high PLQY of 96% and EQE of 20.1% for the near-infrared PeLEDs, approaching to the record EQE of 21.6% for a near-infrared PeLEDs based on 3D FAPbI$_3$ perovskite.[60] By using 1,4-bis(aminomethyl) benzene molecules as bridging ligands in the Dion-Jacobson (DJ) quasi-2D

perovskites, the formation energy is dramatically improved, in comparison to the generally used PEA based RP quasi-2D perovskites. The longest half-lifetime until now was reported to be 100 h, despite its moderate EQE of 5.2% for a near-infrared PeLEDs, which may provide a new strategy to improve the operational stability of PeLEDs.[2b]

The charge funneling efficiency was found to corelate with the crystal orientation, which could be tuned by the solvent of quasi-2D perovskite precursor solution for an efficient green quasi-2D perovskite LED with an EQE of 11.5%.[101] Moreover, the charge transfer and the crystallization was enhanced through the modulation of spacer cations, similar to the widely reported strategy for improving the photovoltaic performance based on quasi-2D perovskites. For instance, dual spacer cations of the phenylbutylammonium (PBA) and the propylammonium (PA) were used to substitute the commonly used PEA cation to achieve a high PLQY of 89% and an EQE of 15.1% for green PeLEDs.[102] Through further bulk and interfacial defects passivation, the EQE of the green quasi-2D PeLED is further improved to 19.1%.[103] It should be noted that the rational design of bulky ammonium salts as spacer cations in quasi-2D perovskites ought to be scrupulous. For instance, the singlet and triplet exciton behavior that is fundamental to the design of efficient organic LEDs but is rare report in PeLEDs should be

considered. Figure 7A shows the crystal structure of quasi-2D perovskites for green LED applications, in which the excitons will be tightly confined at the inorganic well layer. Figure 7B shows its corresponding energy structure and exciton decay dynamics in which the inorganic [PbBr$_6$]$^{4-}$ layer has a Γ_5 singlet state at 3.01 eV and two triplet states of Γ_1 and Γ_2 at ~2.99 eV.[104] The energy gap between the singlet state and the triplet state is extremely small and even could be thermally activated at room temperature. The singlet excitons generated in the quantum well can efficiently transfer via Forster energy transfer over long distances, whereas triplet excitons transfer via Dexter pathways over a short distance. Therefore, in a recent report, the quasi-2D green PeLEDs with PEA spacer cation possessing a high triplet energy level (3.3 eV) could be warranty of efficient carrier transfer based on the funnel model to achieve a high EQE of 12.4%. In contrast, the energy of the lowest excited triplet state of the NMA spacer cation is 2.4 eV, 0.4 eV lower than the two triplet states of Γ_1 and Γ_2 in the inorganic [PbBr$_6$]$^{4-}$ layer. Therefore, if using the NMA as the spacer cation in green-quasi-2D perovskite LEDs, considerable nonradiative recombination would not be avoided, resulting in a low EQE of 3.4%.[106]

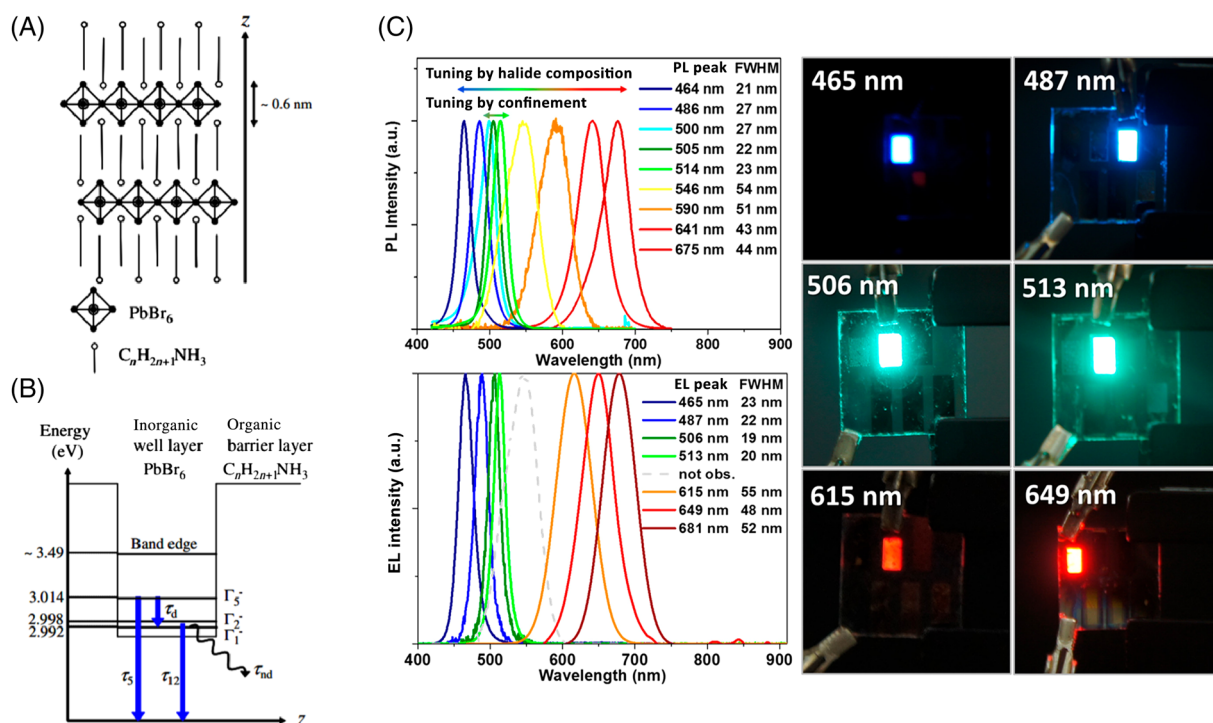Compared to the improved performance and stability of near-infrared, red, and green LEDs based on the quasi-2D

FIGURE 7 Illustration of (A) lattice structure, (B) energy structure, and exciton decay dynamics of (C$_n$H$_{2n+1}$NH$_3$)$_2$PbBr$_4$ quasi-2D perovskite. Reproduced with permission from Reference 104. Copyright 2008, American Physical Society. (C) Normalized PL spectra of BA$_2$Cs$_{n-1}$Pb(Cl$_x$Br$_y$I$_{1-x-y}$)$_{3n+1}$ perovskite thin films, EL spectra, and photograph of the corresponding PeLEDs. Reproduced with permission from Reference 105. Copyright 2018, American Chemical Society

perovskites, the blue quasi-2D perovskites-based LEDs still suffers unsatisfactory device performance. Improving the performance of blue PeLEDs is extremely significant for developing full-color displays and white-light illuminations. The blue PeLEDs can be obtained through incorporating Rb^+ and Cs^+ into quasi-2D perovskites with an EQE of 1.35%.[107] Through the Cl insertion into quasi-2D perovskites and optimization of the radiative recombination zone, the EQE of corresponding PeLEDs was dramatically improved to 5.7%.[108] By incorporating both the Cs^+ cation and the Cl^- halide ion into quasi-2D perovskites, the EL peak and the light emission of corresponding PeLEDs could be tuned from red to blue (Figure 7C).[105] The highest EQE values are 6.2% (465 nm),[105] 6.3% (478 nm)[109] and 12.1% (488 nm)[110] for current state-of-the-art blue PeLEDs fabricated using quasi-2D perovskites. However, the spectral stability of blue PeLEDs is poor and an undesirable shift (over 7 nm) toward the longer wavelength under operating conditions is generally observed due to the Cl ion migration and the multi-phase separation. Sargent et al. ameliorated this issue by dynamic treating the quasi-2D perovskite with organic chlorides.[111] The organic chlorides in situ immobilized Cl vacancy and formed hydrogen bonds with quasi-2D perovskites to inhibit phase separation. The blue PeLEDs were achieved with an EQE of 5.2% and an operating half-lifetime of 90 min.

5.2 | 2D/3D perovskite heterostructure for PeSCs and PeLEDs

The 2D perovskites have a pure one-layer perovskite in the film, while quasi-2D perovskites are mixtures of different perovskite layers in the film.[112] Since the 2D/3D and quasi-2D/3D perovskites have similarities in both structure and working mechanism, we overview the development of PeSCs and PeLEDs based on both 2D/3D and quasi-2D/3D structures in this section.

5.2.1 | PeSCs

The merits of superior device stability based on 2D perovskites have attracted interest in assembling 2D perovskites and 3D counterparts to form 2D/3D heterostructures. Two main strategies have been developed to form the 2D/3D perovskite heterostructure. One method is depositing 2D or quasi-2D perovskites on 3D perovskites by the capping mode. Another approach is the in-situ growth of 2D or quasi-2D perovskites in a 3D perovskite host by an interspersing mode.

The capping mode takes full advantage of the moisture stability of 2D or quasi-2D perovskites to protect the 3D perovskite underlayer from the direct exposure to humid environment. As demonstrated in Figure 8A, the 2D/3D or quasi-2D/3D perovskite heterostructure is generally realized through the post-treatment of a 3D perovskite layer with ammonium salts.[113] The formation of the 2D/3D perovskite heterostructure was confirmed by the high-resolution TEM image showing different diffraction lattices for the 2D perovskite capping layer on the 3D perovskite (Figure 8B).[114] Also, the grazing incidence XRD was employed to elucidate the crystallization process for the 2D/3D perovskite heterostructure. Docampo and co-workers used PEA to post-treat the 3D perovskite and formed a thin layer of quasi-2D $PEA_2MA_2Pb_5I_{16}$ perovskite onside to form the 2D/3D heterostructure. As shown in Figure 8C, both diffraction patterns display the broad Debye–Scherrer rings as a representative of the 3D perovskite host. The labeled ring pattern centered at $q_r = 0$ Å^{-1} corresponds to strongly oriented crystal planes parallel to the substrate, indicating the formation of 2D perovskites.[115] The $PEA_2MA_2Pb_5I_{16}$ quasi-2D perovskite had mutual effects that reorganized and shielded the $MAPbI_3$ underlayer. Such a bilayer configuration demonstrated an efficiency of 14.94% with a benign stability that could retain 76% of its initial efficiency for 19 days in humid air (70% RH). Apart from the quasi-2D perovskite, the thin layer of 2D AVA_2PdI_4 perovskite, where AVA is the amino valeric acid cation, was explored to self-assemble on the 3D $MAPbI_3$ perovskite.[15] A high efficiency in that era of 14.6% for small area cells (0.64 cm^2) and 12.71% for 10 × 10 cm^2 solar module was achieved based on the 2D/3D architecture. The module showed decent stability when it worked at short-circuit conditions under one-sun light illumination and 55°C thermal stresses for 1 year. The integration of multi-phase 3D perovskites with 2D or quasi-2D perovskites should display more satisfactory photovoltaic performance and stability. For instance, PEAI solution was dynamically spin-coated on the 3D $Cs_{0.1}FA_{0.74}MA_{0.13}PbI_{2.48}Br_{0.39}$ (CsFAMA) perovskite to form the 2D/3D heterostructure to achieve a high efficiency of 20.1%.[118] The PEA_2PbI_4/CsFAMA PeSCs exhibited robust durability, which can survive in air (30%–60% RH) for 60 days and maintain 80% of its initial efficiency under the MPP-tracking for 800 h. The BA^+ was used to substitute the PEA^+ to form quasi-2D $BA_2MAPb_2I_7$ perovskite. The quasi-2D $BA_2MAPb_2I_7$ perovskite efficiently passivated the surface trap centers of the 3D CsFA perovskite and remarkably enlarged the V_{OC} of 1.31 V that is the highest V_{OC}-to-bandgap ratio report so far.[119] Most of quasi-2D perovskites formed relying on relatively weak inter-well van der Waals bonds between hydrophobic organic moieties of ligands and such weak bonds post potentially risks on the stability. Recently, ligand-4-vinylbenzylammonium was used to constitute well-ordered perovskite quantum wells atop a 3D CsFAMA perovskite layer. The vinyl group of such ligand
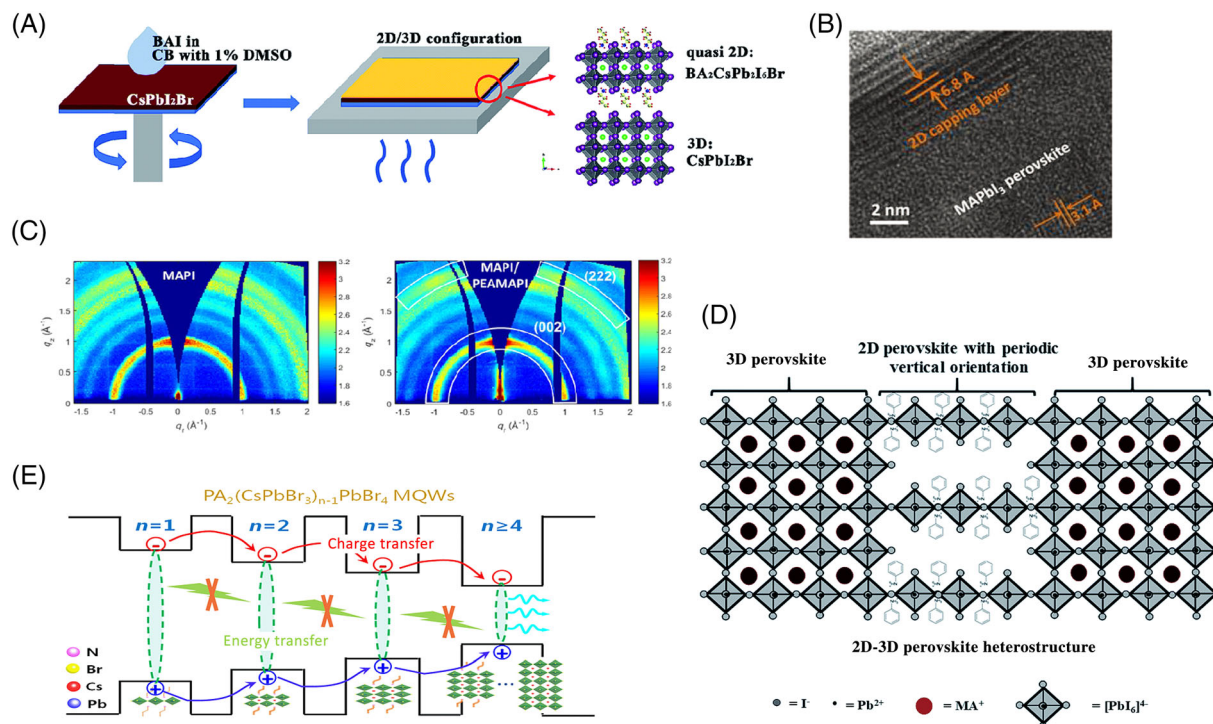
FIGURE 8 (A) Schematic illustrations of the fabrication of 2D/3D heterojunction in the capping mode. Reproduced with permission from Reference 113. Copyright 2019, The Royal Society of Chemistry. (B) Magnified TEM images of the 2D/3D layered heterostructure perovskite film. Reproduced with permission from Reference 114. Copyright 2020, John Wiley and Sons. (C) GIWAXS analysis for the 3D perovskite (left) and 2D/3D perovskite heterojunction (right). Reproduced with permission from Reference 115. Copyright 2016, American Chemical Society. (D) Schematic illustrations of the self-assembled 2D–3D perovskite structure synthesized by the interspersing mode. Reproduced with permission from Reference 116. Copyright 2020, The Royal Society of Chemistry. (E) The electronic band structure of the 2D–3D perovskite heterojunction. Reproduced with permission from Reference 117. Copyright 2018, Elsevier

was activated using UV-light to photochemically form covalent bonds among quasi-2D perovskites.[120] The UV-cross-linked 2D/3D perovskite device exhibited a high efficiency of 20.4% and maintained over 90% of its beginning efficiency when aged in air with the 30% relative humidity for 2300 h.

The 2D/3D perovskite heterostructure in the interspersing mode is realized through directly introducing the bulky ammonium salts in the perovskite precursor and form 2D or quasi-2D perovskites as nanoplates embedded in 3D perovskite crystals. Figure 8D shows the crystallographic connectivity between the quasi-2D and the 3D perovskites synthesized by the interspersing mode.[116] The first work on such a topic was reported by Snaith et al., in which they introduced n-BA$^+$ into the 3D FA$_{0.83}$Cs$_{0.17}$Pb(I$_y$Br$_{1-y}$)$_3$ perovskite precursor solution.[121] Since the perovskite films with 2D/3D heterostructure exhibit the typical quantum-well electronic configuration as shown in Figure 8E,[117] the carrier trapping and recombination can be alleviated at grain boundaries so that the carrier lifetime was increased, contributing to a stabilized power output of 17.3% and 19.5% for the wide-bandgap perovskite and low-bandgap perovskite, respectively. The quasi-2D/3D perovskite in the interspersing mode maintained 80% of its original efficiency for 3880 h for

the encapsulated device operating at open-circuit condition in air (45% RH). Such quasi-2D/3D system was then systematically investigated by controlling the content of BA cations in the precursor. It was found that the appropriated content of quasi-2D perovskites could help to improve crystallinity and appear to passivate grain boundaries, thus enhancing charge-carrier mobilities for an ultra-long carrier-diffusion length up to 7.7 μm.[122] Such quasi-2D/3D heterostructure perovskite film was further treated using molecule passivation and recorded a high efficiency of 20.62%.[123] Another widely used bulky cation, PEA$^+$, was also introduced in the phase-pure 3D FAPbI$_3$ perovskite precursor by Yang et al.[124] The 2D PEA$_2$PbI$_4$ perovskite spontaneously formed at grain boundaries to suppress ion migration to output a high stabilized efficiency of 20.64%. Both outstanding shelf lifetime and operational stability for the 2D/3D heterostructure devices were observed. Motivated by these developments, the low toxic bismuth-based 2D perovskite with small cations, MA$_3$BiI$_9$ was tentatively embedded in the 3D MAPbI$_3$ perovskite to enhance the efficiency to 18.97% from 16.83%. In addition, long-term shelf lifetime was observed for the optimal MA$_3$BiI$_9$-MAPbI$_3$ 2D/3D heterostructure perovskite device.[125] In addition, Wang

et al. fabricated a 2D-quasi-2D-3D hierarchy structural Sn-based perovskite by using pseudohalogen NH_4SCN as a mediator to separate the nucleation and growth of perovskite. The 2D perovskites at the film surface acted as a shield to prevent the oxidation of the internal Sn-based 3D perovskites, significantly enhancing the device lifetime.[126]

5.2.2 | PeLEDs

The strategies of potential or spatial confinement either using the quasi-2D multi-quantum-well structure or reducing the grain size have boosted the rapid development of PeLEDs. One inevitable issue in these potential or confinement structures is the increased surface-to-volume ratio and multiphase interfaces, generating the risk of a high degree of surface or interface defect states. Although these defects are electronically benign or inactive, which exerts benign influence on the performance of high-efficiency PeLEDs, they are critical to the environmental and operational stability of PeLED via ion migration or defects induced film degradation.

Very few reports were reported to mitigate such drawbacks using the 2D/3D heterostructure perovskites film until a recent breakthrough was made by Yang et al. through spin-coating PEA solution on 3D $FA_{0.98}Cs_{0.02}PbI_3$ perovskite to induce the formation of the 2D PEA_2PbI_4 perovskite.[127] By quantitatively controlling the concentration of the spin-coated PEA solution, only a small amount of FA^+ in the 3D perovskite was substituted by the PEA^+ to form surface-2D/bulk-3D hetero-phased perovskite nanograins. The TEM images shown in Figure 9A confirmed the spontaneous formation of the surface-2D perovskite phase on the 3D counterpart rather than the generally investigated quasi-2D RP perovskites for LED applications. They carefully compared the carrier dynamics in such 2D/3D structure with the commonly used 3D perovskite nanograins and quasi-2D perovskites. The spatially resolved electrical properties of the perovskite film was characterized by the conductive atomic force microscopy (c-AFM) as displayed in Figure 9B. The spatial difference in charge carrier conduction was puny, but the electrical properties of quasi-2D perovskites exhibited large grain-to-grain spatial inhomogeneity due to the multiphase in nature with disparate charge transporting capabilities of quasi-2D perovskites. Furthermore, the carrier recombination process was found to be dependent on the form of the perovskite film. As shown in Figure 9C, quasi-2D perovskites and surface-2D/bulk-3D perovskites exhibited shorter and longer PL lifetimes, respectively, than 3D perovskites under a lower carrier density (10^{15} cm^{-3}). In the range of higher excitation carrier densities (10^{16} cm^{-3}), the PL lifetime of surface-2D/

bulk-3D perovskites turned to be shorter than 3D perovskites. This difference indicated that the quasi-2D perovskites presented both strong monomolecular trapping and bimolecular radiative recombination, which was further confirmed by the calculated trap-mediated recombination coefficient A_{trap} and bimolecular radiative recombination coefficient B_{rad} (Figure 9C). By contrast, the surface-2D/bulk-3D perovskites possessed a dramatically decreased A_{trap} but a significantly increased B_{rad}. Therefore, the surface-2D/bulk-3D heterostructure perovskite could reduce trap densities and enhance the radiative recombination efficiently. As measured, the near-infrared PeLEDs based on the surface-2D/bulk-3D heterostructure perovskite exhibited an EQE of 7.7% in together with an improved operational stability. In specific, the surface-2D/bulk-3D PeLED could maintain the initial radiance upon 100 cycles of current–voltage scanning and 100 h, while PeLEDs based on both the 3D and the quasi-2D perovskite declined rapidly within 30 cycles and dropped rapidly within 30-min testing (Figure 9D,E). Although the performance of PeLEDs fabricated using the surface-2D/bulk-3D perovskite was moderate compared with those advanced PeLEDs (∼20% for near-infrared PeLEDs) reviewed in previous chapters, the operational stability is a huge breakthrough. Further works are supposed to improve the performance and stability based on such surface-2D/bulk-3D heterostructure.

Similar to PeSCs, the 2D/3D PeLEDs were also fabricated in an interspersing mode through in-situ growth of 2D perovskites in the 3D perovskite host. Zeng et al. introduced the GABr in the 3D perovskite to form a self-organized 2D/3D perovskite.[128] They found the energy cascade was boosted in the 2D/3D perovskite structure to induce energy transfer from the wide 2D perovskite to 3D perovskite, which enhanced the radiative recombination and density of carriers. Profiting from the optimized energy cascade, a blue PeLED (492 nm) exhibited a high EQE of 8.2% for 2D/3D perovskite structure as compared with the 3D perovskite with an EQE of 1.5%. The carrier density distribution in 2D/3D PeLEDs was capable to stabilize the EL spectra and operational stability.

5.3 | PeSCs and PeLEDs based on 0D/1D@host assembling perovskite matrix

5.3.1 | PeSCs

Initially, the QDs embedded in a high-dimensional perovskite host were focused on the near-infrared PeLEDs were fabricated and exhibited an EQE and SnS QDs.[129] It was found that the perovskite nucleation process was influenced by specific crystal planes of
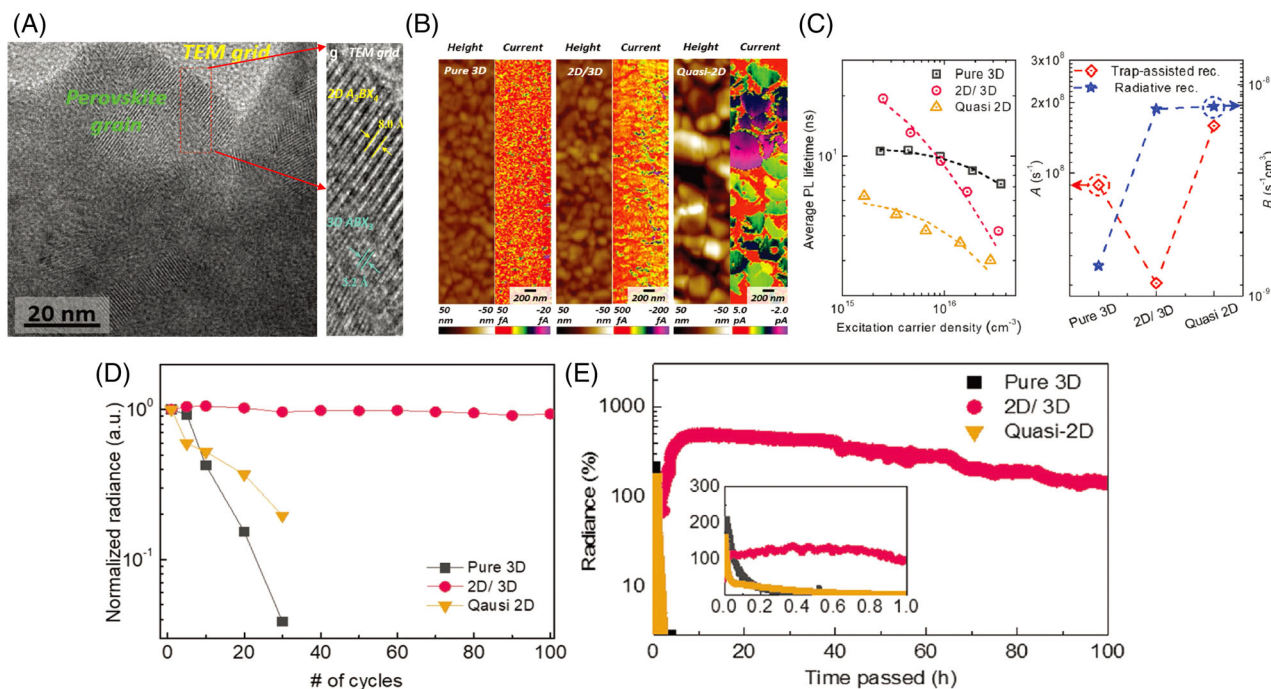
FIGURE 9 (A) TEM images of the surface-2D/bulk-3D heterophased perovskite grains. (B) Atomic force microscope topographic and electrical current mapping of pure 3D, surface-2D/bulk-3D, and quasi-2D perovskite films. (C) Excitation carrier density dependency of average PL lifetime, and the trap-mediated monomolecular recombination coefficient A, and the intrinsic bimolecular radiative recombination coefficient B. (D) Evolution of radiance according to the number of current–voltage scan cycles. (E) Evolution of radiance according to time passed under a constant voltage (initial radiance ≈ 10 W sr^{-1} m^{-2}) of LEDs with pure 3D, surface-2D/bulk-3D, and quasi-2D perovskites. (A)–(E) Reproduced with permission from Reference 127. Copyright 2019, John Wiley and Sons

embedded chalcogenide QDs. The heteroepitaxy-atomically aligned growth of perovskites on the selected plane of chalcogenide QDs was observed through quantitatively controlling the composition of perovskites and the quantity of chalcogenide QDs within the perovskite matrix. Lattice anchoring purpose were thereby achieved to dramatically improve the stability of the hybrid perovskite-QDs films.[129a,d] The embedded chalcogenide QDs were also found to reduce the energy barrier for efficient carrier hopping within the hybrid film in comparison with individual counterparts.[129a,c] Thanks to the lattice anchoring and the fast carrier hopping, the optoelectronic performance of chalcogenide QDs@ perovskite matrix was greatly promoted. For example, PeSCs with efficiencies up to 19% have been reported based on PbS QDs@ MAPbI$_3$ matrix.[129b] Although the photovoltaic performance of PeSCs was improved with QD incorporation, it still far lags behind those advanced PeSC devices with over 20% PCE. This large discrepancy is because PbS QDs could efficiently extract carriers from the large bandgap perovskite to the low bandgap PbS QDs when the PbS QDs is minority. However, if PbS QDs is heavy loaded, perovskite would fill PbS QDs voids so that charge carriers have to surmount a higher barrier to transfer outside. If decreasing the loading of PbS QDs,

the stability improvement would be deteriorated. In addition, in order to realize the heteroepitaxy growth of the perovskite on the PbS plane, the composition of the perovskite, such as I/Br ratio should be strictly controlled for the sake of lattice matching and anchoring between PbS QDs and perovskites.[129a] Nevertheless, the halide ratio is extremely significant to optoelectronic properties and stability of perovskite-based devices.[130] In a word, the balance between the perovskite nucleation and growth and the charge transfer among the hybrid matrix should be considered and optimized for the chalcogenide QDs incorporation.

Although the optoelectronic performance of devices based on chalcogenide QDs@ perovskite matrix is not satisfactory, the concept of borrowing the unique optoelectronic properties of QDs to influence the growth of perovskites and the carrier dynamics within the matrix is interesting. Compared with chalcogenide QDs, the perovskite QDs incorporation would be more promising if considering the latticing matching, homoepitaxy growth, and better chemical compatibility between perovskite QDs and perovskite matrix. However, until now, the related reports on those topics are not as plentiful as chalcogenide QDs incorporation. The lack of research on such topics can be ascribed to the difficulty of the chemical

incorporation of synthesized perovskite QDs within the perovskite matrix because the perovskite compounds are extremely susceptible to polar solvents which are generally used for dissolving perovskite precursors.[31,74]

Currently, a few research works explored the structural assembling between 0D, 1D, and QDs and relatively higher dimensional perovskites (2D and 3D) through using the stoichiometric modulation of added precursors. For instance, Jen et al. reported the formation of a heterojunction of 0D Cs_4PbI_6 and 3D $CsPbI_3$ by tuning the stoichiometry of CsI and PbI_2 to realize a high efficiency PeSCs (16.39%) with a 500 h storage shelf-lifetime (Figure 10A,B). the embedded 0D Cs_4PbI_6 perovskite played the role of molecular locking to improve the activation energy barrier of the matrix as depicted in Figure 10C, and thus stemming the transition of active α-$CsPbI_3$ phase to non-active γ-$CsPbI_3$ phase.[131] Instantaneously, $CsPbBr_2Cl$ PeQDs were introduced during the formation of the 3D perovskite film to distribute QDs elements into the host but leave organic ligands on the surface.[132] The extra elemental additions filled the defect sites to narrow the band-tail electronic states so that a high efficiency of 21.5% was obtained (Figure 10D,E). Simultaneously, the self-assemble organic ligands rendered the matrix a hydrophobic surface to block the moisture penetration and the escape of MA^+, prolonging the operational lifetime of PeSCs (Figure 10F,G). The strategy of simultaneous elements compensation and surface hydrophobization is valid for the optoelectronic performance improvement of PeSCs but leaves the issue that whether QDs still exist or have been dissolved in the host. Similarly, multiple cations PeQDs ($Cs_{0.05}[MA_{0.17}FA_{0.83}]_{0.95}PbBr_3$) were introduced into the 3D perovskite host to offer the dual functions of 1) interdiffusion of cations and anions from PeQDs to occupy the ionic vacancies at the surface and grain boundaries of perovskite host; and 2) leaving the hydrophobic long ligands from PeQDs to form low-dimensional perovskites on the surface to impart ameliorated moisture tolerance.[133] In addition, Zhu et al. referred to the cap function of 2D perovskites in the 2D capped 3D system and coated 0D PeQDs on the surface of 3D perovskites.[134] The coated $CsPbBr_3$ PeQDs effectively suppressed surface imperfections of the 3D perovskite and reduced the non-radiative recombination loss. Therefore, the built-in-potentials determined by the quasi-Fermi level splitting were promoted to achieve a high PCE of 21.03% with a large V_{OC} of 1.19 V for PeSCs.

As shown in Figure 11A, a multi-graded structural assembling (3D-2D-0D) was fabricated via spin-coating 3D $CsPbI_2Br$ bulk film, 2D $CsPbI_2Br$ nanosheet (NSs), and 0D $CsPbI_2Br$ QDs in sequence.[135] Such method induced continuously upshift energy levels of perovskites to optimally align energy levels among the ETL, the multi-graded perovskites and the HTL (Figure 11B), enhancing the carrier extraction and decreasing the interfacial recombination. The continuous upshifted energy levels result in a high J_{SC} of 12.93 mA cm^{-2}. The reduced recombination loss helps to enhance the built-in electric field to obtain a high V_{OC} of 1.19 V and high FF of 80.5%. Consequently, a PCE of 12.39% was obtained for the fabricated PeSCs. Furthermore, such device showed an enhanced stability without any degradation after being stored over 60 days in air with 25%–35% RH at 25°C. For the same purpose of aligning energy level, an internal heterojunction of graded perovskite QDs were formed through spin-coating perovskite QDs with different compositions layer by layer as shown in Figure 11C.[136] The perovskite QDs with different cation ratios of FA/Cs formed the perovskite QDs heterojunction with graded energy level positions (Figure 11D). By virtue of such graded energy level, the photo-generated carriers can be efficiently separated and driven to opposite directions (Figure 11E). This graded energy level aligned structure help to harvest more photogenerated charge carries to increase the J_{SC} for a high PCE up to 17.39%.

During the exploration of assembling 0D perovskites with higher-dimensional perovskites, 1D/3D perovskites assembling was also investigated to further improve the stability of PeSCs. Unlike corner-sharing MX_6 octahedra structures in 3D and 2D perovskites, 1D perovskites have the face-sharing MX_6 octahedra structure that tends to lower the Pb $6s^2$ or Sn $5s^2$ orbital energies dominating the top of the valence bands in perovskites.[137] Therefore, the 1D perovskiteoid exhibit high environmental stability. Fan et al. blended large alkyl ammonium cation salt PZPY into 3D perovskites to induce the 1D $PZPY-PbX_2$ perovskite formation in the 3D perovskite host (Figure 12A) to enhance the cycling stability of PeSCs.[138] As shown in Figure 12C, with the introduction of the 1D perovskite, the perovskite matrix PeSCs could maintain its initial efficiency during the test iterated in a large temperature range. The pronounced cycling stability of the 1D@3D perovskite matrix was stemmed from the better structural flexibility of 1D perovskite (Figure 12B), as compared with the densely packed 3D perovskite, supporting the stress relaxation and defects self-healing within the hybrid perovskite matrix. The same group further optimized the cation salt by using bipyridine (BPy) to form the 1D perovskite which is well-lattice-matched with the 3D perovskite host (Figure 12D). Furthermore, the structurally flexible 1D perovskite alleviated the ion migration to hold up the whole 3D perovskite framework. As shown in Figure 12E,F, the corresponding PeSCs based on 1D@3D perovskites exhibited decent device efficiency (21.18%) with superior stability against moisture, oxygen, and light.[55] However, the intrinsic
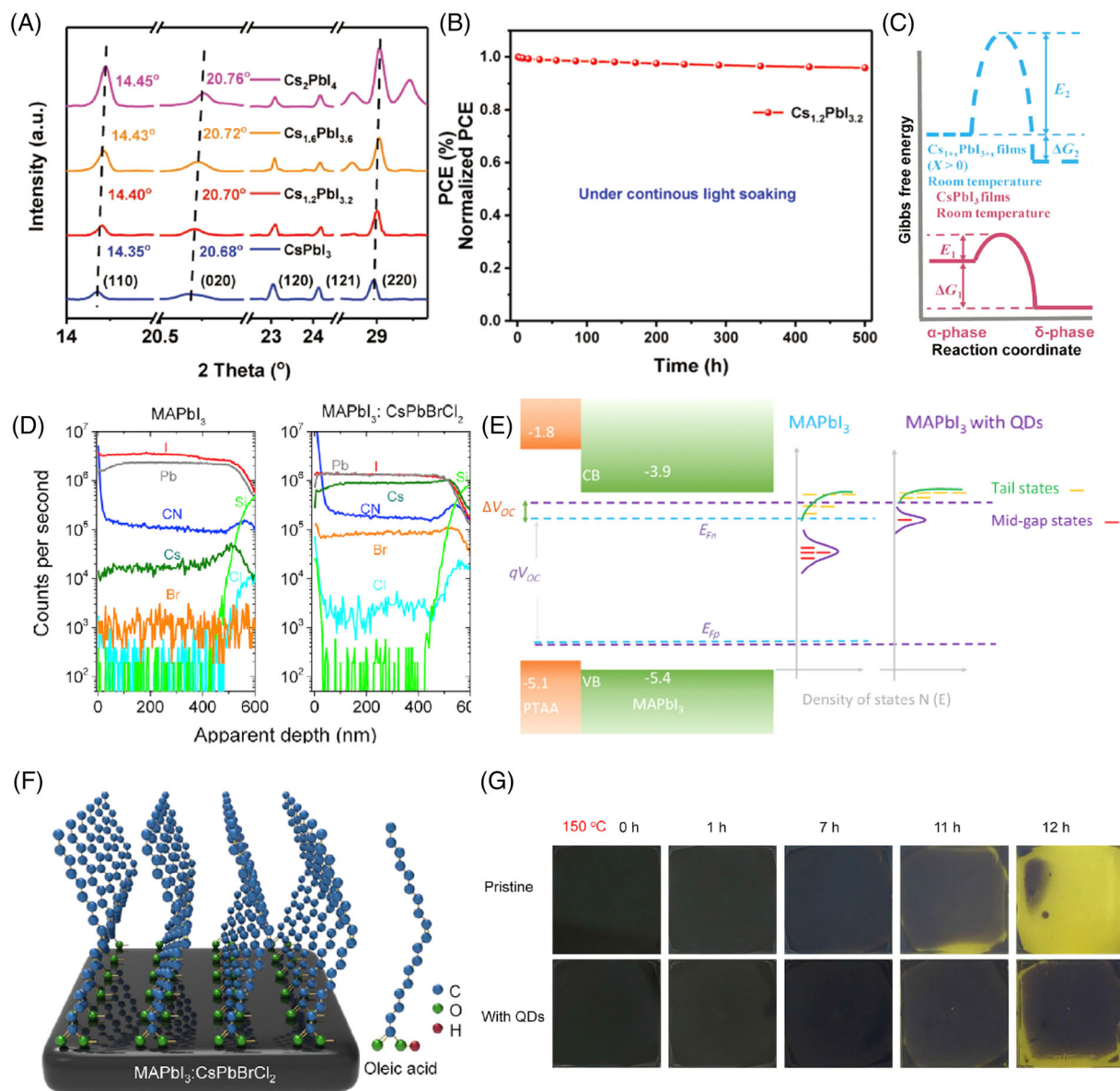
FIGURE 10 (A) XRD patterns of $Cs_{1+x}PbI_{3+x}$ films. Cs_4PbI_6 QDs was formed through stoichiometric modulation of CsI and PbI_2. (B) Light-soaking stability measurement of the device under continuous 1 sun illumination (100 mW cm^{-2}) at room temperature in a nitrogen glovebox. (C) Gibbs free energy and reaction coordinate diagram of $Cs_{1+x}PbI_{3+x}$ films. (A)–(C) Reproduced with permission from Reference 131. Copyright 2019, John Wiley and Sons. (D) Depth-dependent elemental distribution measured by SIMS for the pristine $MAPbI_3$ film and the film with 0.25 wt% of $CsPbBr_2Cl$ QDs in anti-solvent. (E) Schematic illustration of how doped $CsPbBr_2Cl$ QDs influence the tail states and mid-gap states of the perovskite layer. (F) Schematic illustration of the uniform elemental distribution across the $MAPbI_3$ film and self-assembly of the OA molecules on the surface of the $MAPbI_3$ film. (G) Photographic images of $MAPbI_3$ films without QDs and with 0.25 wt% QDs under 150°C for different time intervals in ambient conditions with 70% ± 5% humidity. The size of films is 15 × 15 mm. (D)–(G) Reproduced with permission from Reference 132. Copyright 2019, Elsevier

insulating nature of the organic cations surrounding the face-sharing octahedra in 1D perovskites constrains the one-direction charge carrier transfer. In order to improve the carrier transfer between the face-sharing octahedra, an in-situ cross-linking propargylammonium (PA$^+$) was introduced through a mild thermal treatment to form polymerized groups surrounding the 1D perovskitoid and formed a thin cross-linked 1D perovskite on the top of

3D perovskite. On one hand, the cross-link 1D perovskite exhibits a better carrier transport at the interface. On the other hand, the cross-linked PA$^+$ was illustrated to have the capability to release residual tensile stress. The better charger transfer across the 1D perovskite and 3D perovskite interface and the release of tensile stress benefit the device stability so that a maintained 93% of the initial efficiency (21.19%) was recorded under MPP tracking for
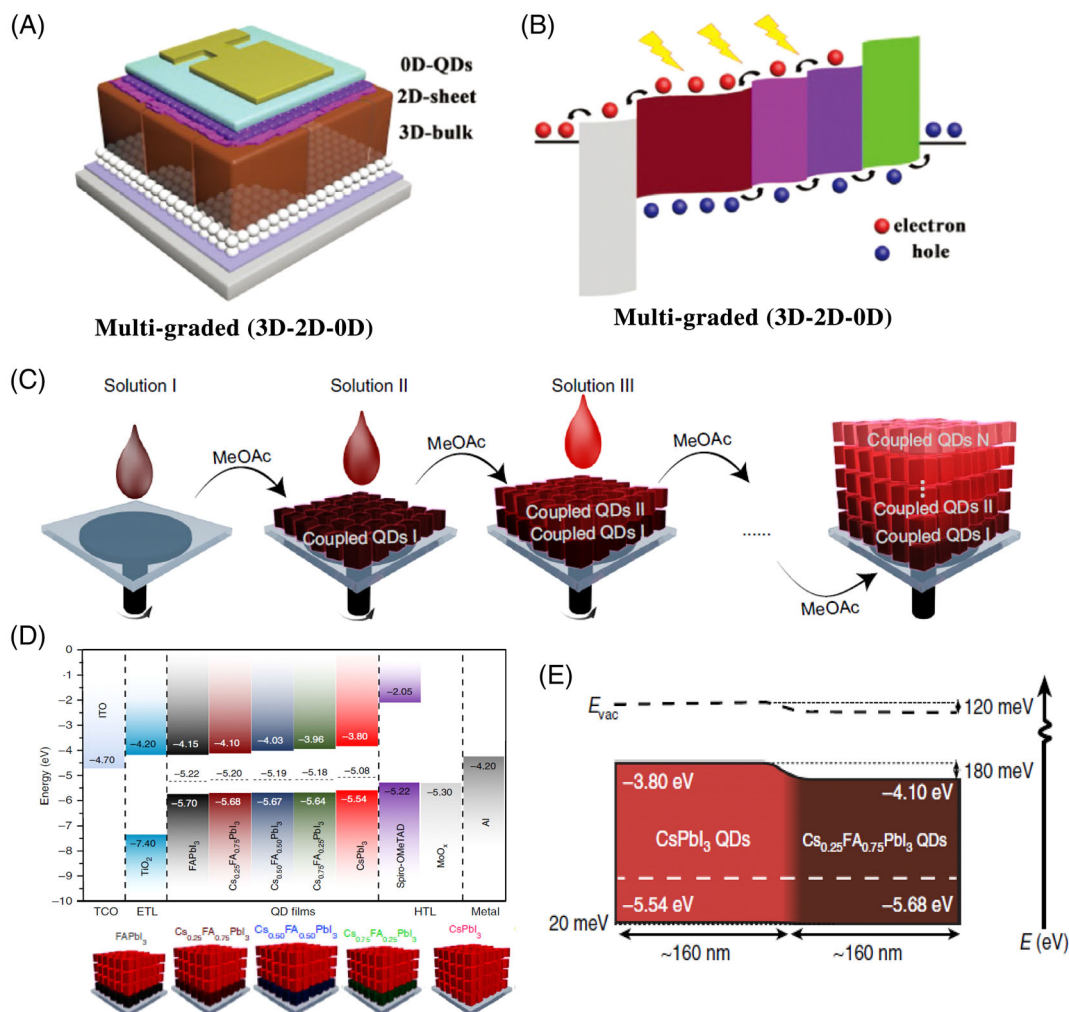
FIGURE 11 (A) Schematic structures of devices without and with a graded interface and (B) energy-level diagram and carrier-transport mechanism in multi-graded $CsPbBrI_2$ PeSCs. (A)–(B) Reproduced with permission from Reference 135. Copyright 2018, John Wiley and Sons. (C) Schematic overview of layer-by-layer assembly showing a perovskite QD film composed of different layers of QDs. MeOAc treatment is carried out between the deposition of different QD layers to remove the native oleate ligands and to render the deposited QDs insoluble in the solvent. (D) Energy band positions for perovskite QD compositions and contact layers considered in the work. (E) Energy level diagram of the heterostructure film. From the alignment, electrons are driven to the FA-containing side with a conduction band offset of 180 meV, while holes have a small (20 meV) offset driving holes toward $CsPbI_3$. (C)–(E) Reproduced under the terms of the Creative Commons CC BY license from Reference 136. Copyright 2019, Springer Nature

3350 h.[16a] Table 1 has summarized the development of PeSCs based on perovskites with structural assembling engineering.

5.3.2 | PeLEDs

Similar to the development of PeSCs, the initially selected QDs to assemble with high-dimensional perovskites for PeLEDs application were the chalcogenide QDs.[129c,142] Recently, PeQDs assembled with quasi-2D perovskites were tentatively applied in PeLEDs. A mesoscopic film architecture (Figure 13A) featuring the graded-size $FAPbBr_3$ PeQDs coupled with 2D $(OA)_2FA_{n-1}Pb_nBr_{3n+1}$

perovskite microplates was designed for efficient green PeLEDs. This unique mesoscopic architecture assembled with PeQDs and 2D perovskites enabled an energy cascade, as revealed in the kinetics of TA signals at 440 and 525 nm in Figure 13B. The 440 nm TA kinetics displayed a faster rising time, distinguishable after 150 fs, versus a much slower rising time (400 fs) for the 520 nm kinetics signal, indicating a slower start-up acceptation of excitons by $FAPbBr_3$ QDs from the 2D $(OA)_2FA_{n-1}Pb_nBr_{3n+1}$ perovskite. Moreover, an internal energy funnel was self-assembled through controlling the grain size of $FAPbBr_3$ PeQDs so that the excitons transferred from the high bandgap 2D perovskite was more efficiently navigated into the low bandgap PeQDs (Figure 13C).[143]
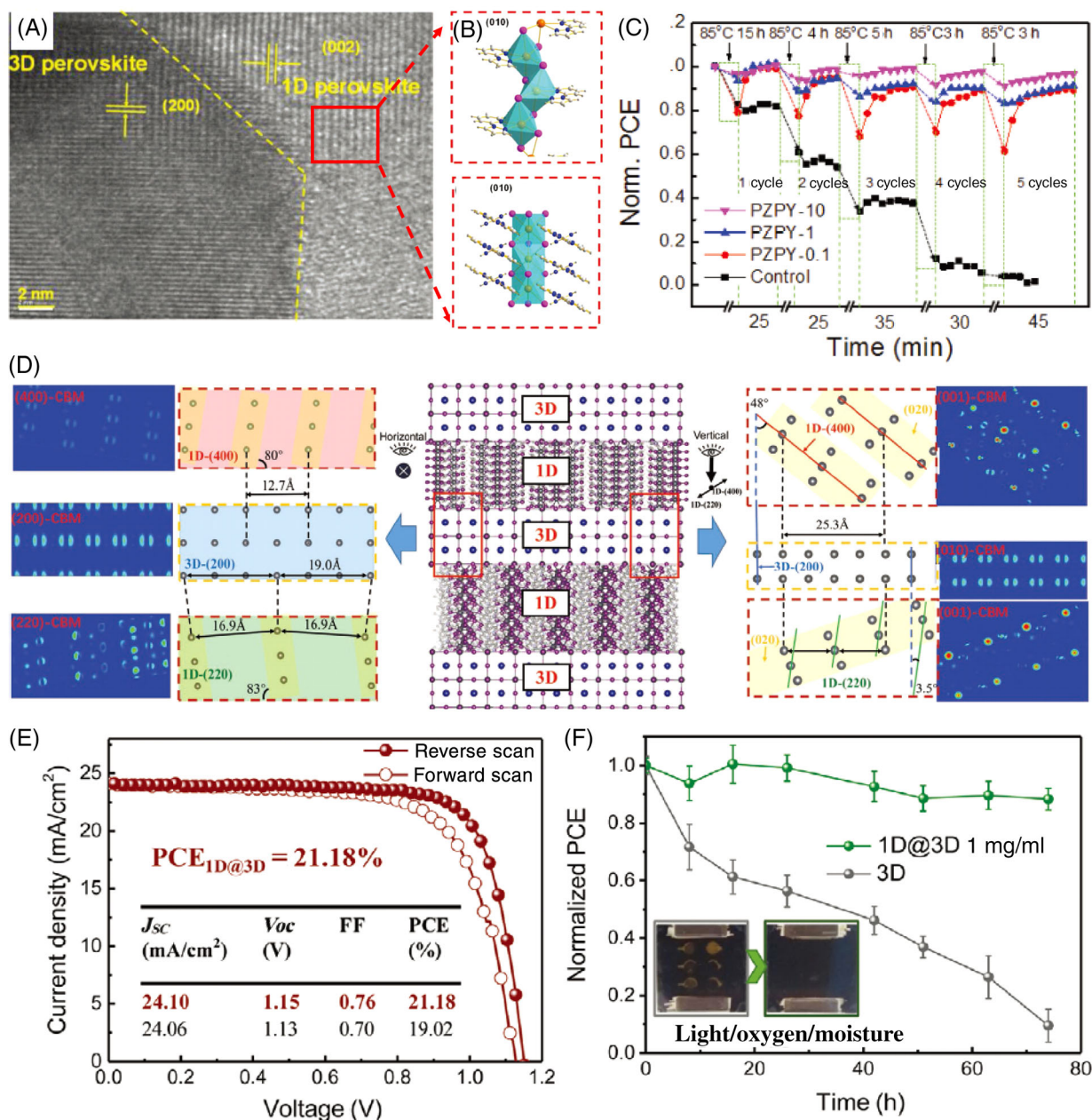
FIGURE 12 (A) High-resolution transmission electron microscopy (HRTEM) image of 1D–3D heterostructure perovskite. (B) Illustration of 1D chain $[PbX_6]^{4-}$ with edge-sharing and face-sharing octahedra. (C) Stability performance of the unencapsulated PVSCs during temperature cycling (25°C–85°C) at 55% RH. (A)–(C) Reproduced with permission from Reference 138. Copyright 2018, John Wiley and Sons. (D) Illustration for the structure of 1D@3D halide perovskite with the calculated CBM and VBM-associated charge density maps. (E) J–V characteristics of the champion PeSC fabricated with the 1D@3D perovskites. (F) Comparison of stability performance of the pristine 3D and 1D@3D hybrid PeSCs. (D)–(F) Reproduced with permission from Reference 55. Copyright 2020, John Wiley and Sons

As expected, the vectoral energy cascade within the structural-assembled mesoscopic structure contributed to high-performance green PeLEDs devices with a high EQE of 13.4% and a high CE of 57.6 cd A^{-1}. Apart from the cascade structural assembling, the attempt of confining PeQDs within the 2D perovskite for PeLEDs application was also successfully conducted recently. Treated with antisolvent dissolved with PABr, the uniform perovskite film comprising quantum-confined

nanoparticles embedded in a majority of quasi-2D phase was obtained.[144] The PeQDs have a relatively a lower bandgap than the quasi-2D counterpart and a scenario was built that excitons could efficiently transfer from the qausi-2D perovskite to PeQDs. Through this method, the highest EQE of 9.5% for the blue PeLEDs was achieved. Although reports on the assembling between 0D or 1D perovskites and 2D or 3D counterparts are not abundant, their mutual combination may be promising

TABLE 1 Summary of the photovoltaic performance of PeSCs based on perovskite matrix with dimensional assembling engineering

Dimension assembling	Type of perovskite	V_{OC} (V)	J_{SC} (mA cm^{-2})	FF (%)	PCE (%)	Shelf lifetime	MPP-stability	Reference
Quasi-2D	$(BA)_2(MA)_3Pb_4I_{13}$ (hot cast)	1.01	16.76	74.13	12.51	2050 h: 70% (light, N$_2$) 10 h: 50% (65% RH)	–	37
Quasi-2D	$(BA)_2(MA)_3Pb_4I_{13}$ (on PTAA)	1.11	17.50	73.29	14.28	1000 h: 97% (dark, N$_2$)	–	91
Quasi-2D	$BA_2(MA_{0.8}FA_{0.2})_3Pb_4I_{13}$	0.999	18.12	70.79	12.81	1300 h: 88% (40%–60% RH)	–	95b
Quasi-2D	$BA_2(MA_{0.95}Cs_{0.05})_3Pb_4I_{13}$	1.08	19.95	63.47	13.68	1400 h: 89% (dark, 30% RH)	–	95a
Quasi-2D	$BA_2(MA_{0.64}FA_{0.34}Cs_{0.02})_4Pb_5I_{16}$	1.13	18.23	69	14.23	–	–	96
Quasi-2D	$(BA)_{1.6}(MA)_{3.4}Pb_4I_{13}$	1.09	17.66	80.20	15.44	85 days: 3% (N$_2$)	–	93
Quasi-2D	$(BA_{0.9}PEA_{0.1})_2MA_3Pb_4I_{13}$	1.182	17.12	76.40	15.46	1200 h: 95% (N$_2$, light) 7000 h: 92% (N$_2$, 85°C)	700 h: 80%	97
Quasi-2D	$3BBA_2MA_{n-1}Pb_nI_{3n+1}$ ($n = 3$ or 4)	1.23	18.22	81.2	18.20	2400 h: 82% (40% RH)	–	90
Quasi-2D/3D	$PEA_2MA_4Pb_5I_{16}$ /MAPbI$_3$	1.08	18.63	73	14.94	19 days: 70% (79% RH)	–	115
Quasi-2D/3D	$BA_2MAPb_2I_7/Cs_{0.17}FA_{0.83}PbI_{1.8}Br_{1.2}$	1.31	19.3	78	19.8%	–	20 h:100% (open-circuit)	119
Quasi-2D/3D	$BA_{0.05}(FA_{0.83}Cs_{0.17})_{0.91}Pb(I_{0.8}Br_{0.2})_3$	1.14	22.7	80	20.6	–	3880 h: 80% (open circuit, encapsulated, 45% RH)	121
Quasi2D/3D	BA_2PbBr_4/FAPbI$_3$ (molecule passivation)	1.10	24.40	76.9	20.62	2208 h: 80% (dark, 40% RH, RT)	–	123
2D/3D	AVA_2PbI_4/MAPbI$_3$	1.054	21.45	70.3	14.6	300 h: 60% (light, Ar, 45°C)	10 000 h: 100% (55°C, short-cicuit)	15
2D/3D	VBA-2D/CsFAMA	1.15	22.5	78	20.2	2300 h: 90% (dark, 30%RH)	–	120
2D/3D	PEA_2PbI_4/CsFAMA	1.15	22.73	79.4	20.75	60 days: 100% (dark, 30-60%RH)	800 h: 90%	118
2D/3D	PEA_2PbI_4/FAPbI$_3$	1.14	24.22	76.6	21.15	60 days: 52% (dark, 25°C, 30%–40% RH)	–	139
2D/3D	$(SBLC)_2PbI_4$/MAPbI$_3$	1.19	22.36	75.7	20.14	30 days: 80.9% (50% RH) 24 h: 80% (85°C, N$_2$) 300 h: 84% (light, N$_2$)	–	114
2D/3D	PEA_2PbI_4/FAPbI$_3$	1.126	24.44	76.5	21.06	1392 h: 98% (dark, 30% RH)	450 h: 80%	124
2D/3D	$MA_3Bi_2I_9$/MAPbI$_3$	1.09	23.03	75.57	18.97	1000 h: 72.34% (30% RH, RT)	–	125
0D@3D	Cs_4PbI_6@CsPbI$_3$	1.09	18.84	80	16.39	500 h:100% (light, N$_2$)	–	131

TABLE 1 (Continued)

| Dimension assembling	Type of perovskite	V_{OC} (V)	J_{SC} (mA cm^{-2})	FF (%)	PCE (%)	Shelf lifetime	MPP-stability	Reference
0D@3D	CsPbBr$_2$Cl@MAPbI$_3$	1.15	23.40	80	21.50	12 h: film stability (150°C, 70% RH)	500 h: 80%	140
0D@3D	CsPbBr$_3$ PeQDs@CsFAMA	1.19	22.95	77	21.03	–	–	134
0D@3D	Cs$_{0.05}$(MA$_{0.17}$FA$_{0.83}$)$_{0.95}$ PbBr$_3$@(FAPbI$_3$)$_x$ (MAPbBr$_3$)$_{1-x}$	1.10	23.82	80.8	21.10	168 h: 80% (85°C, dry air) 1050 h: 92.8% (60% RH, RT)	560 h: 95%	141
0D@2D@3D	CsPbI$_2$Br QDs-NSs-film	1.19	12.93	80.5	12.39	60 days: 100% (25°C, 25%–35% RH)	–	135
Graded 0D	Cs$_{0.25}$FA$_{0.75}$PbI$_3$-CsPbI$_3$	1.20	18.91	76	17.39	–	–	136
1D@3D	TAPbI$_3$@(MA, FAPbI$_3$)	1.08	22.81	77	18.97	1500 h: 92% (20 ± 10%, 20 ± 5°C)	–	137
1D@3D	PbX$_2$-PZPY @CsFAMA	1.08	21.70	77	18.10	35 h: 90% (85°C, 50% RH)	160 min: 90% (5 cycles, 25–85°C, 55% RH)	138
1D@3D	PbI$_2$-BPy@CsFAMA	1.15	24.10	76	21.18	75 h: 90% (light, 50% RH)	–	55
1D@3D	PbI$_2$-cross link PA@CsFAMA	1.11	23.69	80.8	21.19	1500 h: 97% (40%–70% RH, 25–40°C); 840 h: 95.9% (0.8 Sun)	3055 h: 93%	16a
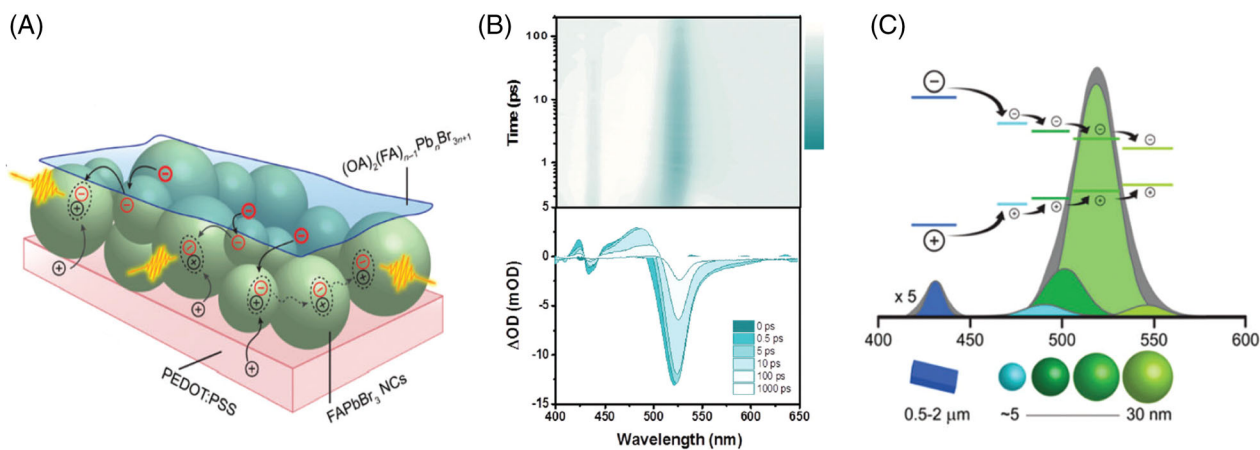
FIGURE 13 (A) Illustrations of energy transfer processes in the perovskite nanocrystal thin film under PeLED device operation condition. (B) TA spectra of FAPbBr$_3$@(OA)$_2$FA$_{n-1}$Pb$_n$Br$_{3n+1}$ composite perovskite film. (C) Illustration to show the energy cascade from 2D perovskite to 0D PeQDs with graded size, where the deconvolution of the steady-state PL spectrum clearly displays the different PL contribution at varying PeQDs sizes. (A)–(C) Reproduced with permission from Reference 143. Copyright 2018, The Royal Society of Chemistry

for the development of PeLEDs, if considering the advantages of PeQDs and perovskite nanorods, in particular their strong quantum confinement for high PLQY.[12,56] The development of PeLEDs with perovskite structural assembling engineering has been summarized in Table 2.

TABLE 2 Summary of properties of PeLEDs fabricated by perovskite structural assembling engineering

Structure assembling	Type of perovskite	EL (nm)	Max EQE (%)	Max CE (cd/A)	L_{max} (cd m^{-2})	Half-lifetime (T$_{50}$)	Reference
Quasi-2D	PEA$_2$MA$_4$Pb$_5$I$_{16}$	760	8.8	–	–	–	99
Quasi-2D	(NMA)$_2$(FA)Pb$_2$I$_7$	800	20.1	–	–	46 h	100
Quasi-2D	(BAB)FA$_{n-1}$Pb$_n$I$_{3n+1}$	787	5.2	–	–	100 h	2b
Quasi-2D	PEA$_2$Cs$_{2.4}$MA$_{0.6}$Pb$_4$Br$_{13}$ (TPPO treatment)	517	14	–	45 230	3.5 h	145
Quasi-2D	(PA/PBA)$_2$FA$_{n-1}$Pb$_n$Br$_{3n+1}$	534	15.1	66.1	8052	–	102
Quasi-2D	PEA$_2$MA$_2$Pb$_3$Br$_{10}$	511.4	9.9	23.46	66 000	25 min	146
Quasi-2D	PEA$_2$FA$_{n-1}$Pb$_n$Br$_{3n+1}$	527	12.4	52.1	–	–	106
Quasi-2D	PEA$_2$FA$_3$Pb$_4$Br$_{13}$	542	11.5	41	–	–	101
Quasi-2D	PEA$_2$(Rb$_{0.6}$Cs$_{0.4}$)$_2$Pb$_3$Br$_{10}$	476	1.35		100.6	14.5 h	107
Quasi-2D	PEA$_2$Cs$_{n-1}$Pb$_n$(Cl$_x$Br$_{1-x}$)$_{3n+1}$	480	5.7	6.1	3780	10 min	108
Quasi-2D	BA$_2$Cs$_{n-1}$Pb(Cl$_x$Br$_y$I$_{1-x-y}$)$_{3n+1}$	487	6.2	~6	3340	–	105
Quasi-2D	PEA$_2$Cs$_{1.6}$MA$_{0.4}$Pb$_3$Br$_{10}$ (DPPOCl treatment)	479	5.2	–	–	90 min	111
Quasi-2D	PEA$_2$Cs$_{n-1}$Pb$_n$Br$_{3n+1}$ (GABr-treatment)	478	6.3	–	200	150 s	109
Quasi-2D	PEA$_2$Cs$_{n-1}$Pb$_n$Br$_{3n+1}$ (TPPCl and LiF treatment)	520	19.1	–	1500	–	103
2D/3D	PEA$_2$PbI$_4$/FA$_{0.98}$Cs$_{0.02}$PbI$_3$	~830	7.7	–	–	100 h: >100%	127
2D/3D	(PEA$_{0.75}$GA$_{0.25}$)$_2$PbBr$_4$/CsPb(BrCl)$_3$	492	8.2	13.1	1003	274 s	128
2D/3D	BA$_2$PbI$_4$/MAPb(I/Br)$_3$	~720	16.8	–	–	47 h	147
0D@2D	FAPbBr$_3$@(OA)$_2$FA$_{n-1}$Pb$_n$Br$_{3n+1}$	525	13.4	57.6	34 480	800 s	143
0D@Quasi-2D	Cs$_x$FA$_{1-x}$PbBr$_3$@PBABr$_2$-(Cs$_{0.7}$FA$_{0.3}$PbBr$_3$)	483	9.5	12	54	250 s	144

6 | CONCLUSION AND PERSPECTIVES

Perovskite materials with the structural modulation and assembling have exhibited adjustable and appealing properties for various optoelectronic applications. In specific, 3D perovskites are suitable for the photovoltaic application due to the small exciton binding energy and excellent carrier mobilities. Low-dimensional perovskites with high exciton binding energy could efficiently reduce the carrier dissociation and are promising for LED applications. The structural modulation of perovskite materials has a significant effect on the stability of perovskite films due to its influence on the enthalpy. Through structural assembling engineering that combining perovskites with different structures within one matrix, the optoelectronic properties and the operational stability of perovskites can be effectively improved for more efficient and stable optoelectronic devices. In this review, the reciprocity relationship between PeSCs and PeLEDs was first elaborated. The optoelectronic

properties of various perovskites based on structural modulation were then discussed. A more vivid and detailed review and discussion were followed premised on these fundamental types of perovskites and structurally assembled perovskites for the application of both PeSCs and PeLEDs. Although various works have reported on perovskite structural modulation and assembling for various optoelectronic devices, there are several key aspects to be resolved before industrialization.

6.1 | Precisely control and plentiful structural assembling engineering

Currently, a series of guidelines have been demonstrated to construct perovskite heterostructures, which could be simply generalized as follows. To form 2D-3D assembled perovskites, including quasi-2D perovskite and the 2D/3D perovskite heterostructure, large or bulky organic cations, such as PEA$^+$, BA$^+$, and PBA$^+$, are usually

introduced into 3D perovskites. The recipe of 2D-3D assembled perovskite system is applicable to the formation of 1D-3D perovskite heterostructure where the 1D perovskite exists in the grain boundaries or on the surface of 3D perovskites. A slight difference between the 1D-3D perovskite heterostructure and 2D-3D perovskite heterostructure is the selection of large organic salts. Propargyl ammonium cation (PA$^+$) and bipyridine (BPy) are widely used as large cations for the formation of 1D perovskites.[16a,55] For the formation of the 0D/3D perovskite structure, one method is incorporating the PeQDs with 3D perovskites.[148] Another approach is tuning the stoichiometry of the precursors between organic cations and metal halides.[131,149] In addition to the perovskite dimensionality modulation, controlling the precursor reactions also can assemble perovskites with different compositions. For example, Peng et al. fabricated $Cs_{0.15}FA_{0.85}PbI_3/Cs_xFA_{1-x}PbI_3$ core/shell heterostructure perovskite by using CsSCN as a reactant to exchange the surface FA cations with Cs. Such core/shell heterostructure perovskite exhibits enhanced stability under atmospheric conditions and high temperatures because the Cs-rich $Cs_xFA_{1-x}PbI_3$ shell can stabilize the perovskite surface.[150] However, how to precisely control the perovskites assembling is difficult. For example, the number of the 2D perovskite layer in quasi-2D perovskites is often undetermined and debatable. If incorporating other structural perovskites with 2D or quasi-2D perovskites, the layer number of the layered perovskite may be disturbed due to the change of its nucleation or crystallization. Likewise, the growth direction of different structural perovskites, for example, the out-of-plane growth of 2D perovskites, epitaxial growth of perovskite host along the wall of 1D perovskites or selected crystal planes of PeQDs, should take attention because the anisotropic optoelectronic properties of perovskites will affect the final device performance directly.

Furthermore, the interface alignment among the multiple phases of perovskites with structural assembling should be optimized, such as the interface within the quasi-2D perovskites as well as 2D/3D heterostructure perovskites, and the interface between the 0D/1D perovskites and their host perovskites. Considering the different optoelectronic properties for disparate phases of the structurally assembled perovskites, theoretical investigations on the dynamics of interfacial carrier transport, interfacial electronic structures, and efficient interfacial alignment modulation methods should be performed.

Apart from the precisely control of the structure and the morphology of perovskites, there is a wide space for selecting the organic cations in the low-dimensional perovskites, such as the bulky organic cations for 2D or quasi-2D perovskites, the ligands for 1D and 0D perovskites. Currently, the chemical interaction between these organic cations and the octahedra units have been widely investigated to build a few

guidelines for the use of organic cations. However, the deeper understanding to build the more general guidelines is needed, such as the effect of the functional groups and chain length on the excitonic states and charge transfer between the donor and acceptor states within perovskites. In order to avoid the conventional strategy of trial-and-error in exploring the organic cations, a few new emerging techniques may be helpful, such as machine learning in combination with first-principles calculations, to assist the development of more suitable organic cations for different perovskite matrix. Based on the further exploration of organic cations, the carrier dynamics in the hybrid perovskite matrix may be more efficient to be controlled to enhance the device performance.

6.2 | Deep photo physics understanding and photon management

Except for the understanding of carriers transfer over the interface between different perovskite phases, the theoretical investigation on the photon recycling in perovskite materials with structural assembling should also be considered. As discussed in the Section 3 of carrier dynamics of perovskites, the photon recycling is a distinct feature for 3D perovskites, which favors the performance of PeSCs and PeLEDs. However, the potential of the photon recycling contributed to the performance improvement has not been fully utilized. For the sake of maximizing the photon recycling effect, the photon management would be an efficient strategy that can be realized through re-optimizing the architecture of perovskite optoelectronic devices and the structure and morphology of perovskites. For example, by introducing special nano- or meso- structured back mirror in PeSCs to improve the photon recycling.[151] Reducing the emissive electrode area and introducing the back mirror layer with a high reflectivity to pump out all photons and direct the photon flux flow.[51] The perovskite materials possess high reflectivity indexes and can be modulated through altering their compositions and structures. By introducing the structural assembling strategy to assemble perovskites in the order of reflectivity indexes, a photon tunnel similar to the carrier transfer cascade in quasi-2D perovskites can be formed to realize the photon recycling function. Although a few works were committed to maximizing the photon recycling in experiment and numerical simulation,[51,151] the device optoelectronic performance still lags behind expectations. Further works regarding the architecture design and structure modulation for structurally assembled perovskites in together with related deep photo-physics understanding are needed to further boost the performance of PeSCs and PeLEDs.

6.3 | Toxicity problem and stability issue

Despite the intensive development of PeSCs and PeLEDs, the toxicity issue of lead has attracted the main concern and a great anxiety for ecologists. The maximum Pb^{2+} content is set at the maximum level of 0.15 and 15 μg/L in air and water, respectively, according to rules and regulations issued by the U.S. EPA.[152] Pb ions, once leaked and washed away, have a larger solubility (K_{sp}) on the order of magnitude of 10^{-8} than that of the toxic Cd ion (10^{-22}).[153] A direct strategy for addressing the toxicity of lead-based perovskites is to prevent the leakage of Pb ions in perovskite materials. For instance, Qi et al. simulated the realistic scenarios in which perovskite devices with different encapsulation methods were mechanically damaged by a hail striking and quantitatively measured the Pb leakage rates under a series of weather conditions.[154] They found that the optoelectronic devices based on the epoxy encapsulation dramatically reduced the Pb leakage rate, in comparison with the glass sheet covering. The reduction of the Pb leakage by epoxy is ascribed to its optimal healing characteristic and superior mechanical strength. A chemical approach by coating of lead-absorbing material on the front and back sides of the device stack was recently demonstrated.[155] The chemicals coated on both sides could swell to absorb the lead, rather than dissolve it, when subjected to sever conditions, therefore retaining the structural integrity for easier collection and recycling of lead after device damage.

In normal operational conditions, if the halide perovskite-based optoelectronic devices can work for a long term, the lead leakage issue would be alleviated drastically. Therefore, improving the stability of optoelectronic devices is a critical way to satisfy requirements for both commercialization and ecological protection. Perovskites with structural modulation and assembling have shown the potential to achieve stable devices, for example, several thousand hours stabilization for PeSCs and several hundred hours half-lifetime for PeLEDs. In together with external engineering methods, such as lead-leakage prevention methods illustrated above and valid encapsulation methods, perovskites materials with the structural assembling approach can be expected to further enhance the device stability. Apart from the widely explored lead-based perovskite, lead-free perovskite materials are also potential candidates to address the issue of the toxicity of lead.[31,32,156] However, the performance of those lead-free based perovskite optoelectronic devices is still incomparable to the lead-based ones and their stability is also challenging. The demonstrated structural assembling strategy would provide tremendous opportunities for lead-free perovskites and more efforts can be invested.

The stability of perovskites is another tough issue in the field of PeSCs and PeLEDs. It is well-known that the 3D organic–inorganic hybrid perovskites are sensitive to the moisture in ambient air.[157] It is agreed that water is one of the major degradation factors for 3D perovskites due to the irreversible reaction between water and perovskites. As a result, optoelectronic devices based on 3D perovskites usually show fast degradation when they are operated under a humid environment. However, for the low-dimensional perovskites, it becomes much difficult for moisture to permeate into perovskite structure because the long-chain cations for low-dimensional perovskites are hydrophobic.[158] Therefore, the low-dimensional perovskites show better humidity stability than their 3D perovskite counterparts. On the other hand, a trace amount of water has been also reported to have a positive effect on perovskites by promoting the nucleation and crystallization of perovskites during the film growth.[159] For example, for 3D perovskites, Zhou et al. found that moisture can enhance the reconstruction process of perovskites by partially dissolving the reactant species and accelerating mass transport within the film, and then exhibited enhanced optoelectronic properties compared with a film grown in dry conditions.[160] For the low-dimensional perovskites. Liu et al. introduced water into the perovskite precursor solution and obtained high-quality 2D perovskite film. Compared to the DMF solvent, water additive can regulate the crystallization process of perovskite because of its lower boiling point and higher vapor pressure.[161] However, the amount of water additive should be carefully controlled. Voids and cracks can be formed when the water content is over 5%, which is mainly due to the decomposition of the hydrate perovskite caused by excessive water.[162] Furthermore, water has been found to facilitate the formation of low-dimensional perovskites. For example, Turedi et al. demonstrated that introducing water on a 3D $CsPbBr_3$ film leads to a direct transformation to a highly emissive 2D $CsPb_2Br_5$ film, which can be explained by a sequential dissolution–recrystallization process induced by water. The post-synthesized 2D film exhibit good thermal and moisture stability.[163] As for the 0D nanocrystals, the addition of a controlled amount of water during the synthesis process would result in improved PLQY and stability. For example, Kim et al. proved that water molecules in perovskite nanocrystals can promote the crystallization by strengthening the bonding between Pb and Br. Consequently, the $CsPbBr_3$ nanocrystals exhibited a PLQY greater than 90% and sustained stability over 35 days.[164] Based on the above analysis, it is arbitrary to conclude whether water is beneficial or harmful to perovskites. More efforts should be made to investigate the degradation mechanisms of perovskite materials and devices which may be triggered by both

ambient environment and device architectures.[10c,165] Advanced encapsulation technologies are also a possible pathway to further develop high-performance perovskite-based optoelectronic devices.[166]

CONFLICT OF INTEREST

The authors declare no conflict of interest.

ORCID

Zhaofu Zhang https://orcid.org/0000-0002-1406-1256
Yuanhang Cheng https://orcid.org/0000-0002-3062-9593

REFERENCES

1. a Stranks SD, Eperon GE, Grancini G, et al. Electron-hole diffusion lengths exceeding 1 micrometer in an organometal trihalide perovskite absorber. *Science*. 2013;342(6156):341-344. b Liu X, Cheng Y, Tang B, et al. Shallow defects levels and extract detrapped charges to stabilize highly efficient and hysteresis-free perovskite photovoltaic devices. *Nano Energy*. 2020;71:104556.

2. a Cheng Y, Yang Q-D, Xiao J, et al. Decomposition of organometal halide perovskite films on zinc oxide nanoparticles. *ACS Appl Mater Interfaces*. 2015;7(36):19986-19993. b Shang Y, Liao Y, Wei Q, et al. Highly stable hybrid perovskite light-emitting diodes based on Dion-Jacobson structure. *Sci Adv*. 2019;5(8):eaaw8072.

3. National Renewable Energy Laboratory Best Research-Cell Efficiency Chart, https://www.nrel.gov/pv/cell-efficiency.html

4. Kojima A, Teshima K, Shirai Y, Miyasaka T. Organometal halide perovskites as visible-light sensitizers for photovoltaic cells. *J Am Chem Soc*. 2009;131(17):6050-6051.

5. Cheng Y, Ding L. Pushing commercialization of perovskite solar cells by improving their intrinsic stability. *Energy Environ Sci*. 2021;14(6):3233-3255.

6. Kim Y-H, Kim S, Kakekhani A, et al. Comprehensive defect suppression in perovskite nanocrystals for high-efficiency light-emitting diodes. *Nat Photonics*. 2021;15:148-155.

7. Tan ZK, Moghaddam RS, Lai ML, et al. Bright light-emitting diodes based on organometal halide perovskite. *Nat Nanotechnol*. 2014;9:687-692.

8. a Kuei C-Y, Tsai W-L, Tong B, et al. Bis-tridentate ir(iii) complexes with nearly unitary rgb phosphorescence and organic light-emitting diodes with external quantum efficiency exceeding 31%. *Adv Mater*. 2016;28(14):2795-2800. b Zhang H, Chen S, Sun XW. Efficient red/green/blue tandem quantum-dot light-emitting diodes with external quantum efficiency exceeding 21%. *ACS Nano*. 2018;12(1):697-704.

9. a Bu T, Liu X, Zhou Y, et al. A novel quadruple-cation absorber for universal hysteresis elimination for high efficiency and stable perovskite solar cells. *Energy Environ Sci*. 2017;10(12):2509-2515. b Liu X, Cheng Y, Liu C, et al. 20.7% highly reproducible inverted planar perovskite solar cells with enhanced fill factor and eliminated hysteresis. *Energy Environ Sci*. 2019;12(5):1622-1633. c Cheng Y, Li M, Liu X, et al. Impact of surface dipole in NiOx on the crystallization and photovoltaic performance of organometal halide perovskite solar cells. *Nano Energy*. 2019;61:496-504. Xie Y, Yin J, Zheng J, Fan Y, Wu J & Zhang X. Facile RbBr interface modification improves perovskite solar cell efficiency. Materials Today Chemistry. 2019;14:100179.

10. a Huang H-H, Shih Y-C, Wang L, Lin K-F. Boosting the ultra-stable unencapsulated perovskite solar cells by using montmorillonite/CH3NH3PbI3 nanocomposite as photoactive layer. *Energy Environ Sci*. 2019;12(4):1265-1273. b Zhang X. Strain Control for Halide Perovskites. *Matter*. 2020;2(2):294-296. c Cheng Y, Liu X, Guan Z, et al. Revealing the degradation and self-healing mechanisms in perovskite solar cells by sub-bandgap external quantum efficiency spectroscopy. *Adv Mater*. 2021;33(3):2006170.

11. Polman A, Knight M, Garnett EC, Ehrler B, Sinke WC. Photovoltaic materials: Present efficiencies and future challenges. *Science*. 2016;352(6283):aad4424.

12. Wei Y, Cheng Z, Lin J. An overview on enhancing the stability of lead halide perovskite quantum dots and their applications in phosphor-converted LEDs. *Chem Soc Rev*. 2019;48(1):310-350.

13. Zhu P, Zhu J. Low-dimensional metal halide perovskites and related optoelectronic applications. *InfoMat*. 2020;2(2):341-378.

14. a Gao P, Yusoff ARBM, Nazeeruddin MK. Dimensionality engineering of hybrid halide perovskite light absorbers. *Nat Commun*. 2018;9:5028. b Grancini G, Nazeeruddin MK. Dimensional tailoring of hybrid perovskites for photovoltaics. *Nat Rev Mater*. 2018;4:4-22.

15. Grancini G, Roldán-Carmona C, Zimmermann I, et al. One-Year stable perovskite solar cells by 2D/3D interface engineering. *Nat Commun*. 2017;8:15684.

16. a Yang N, Zhu C, Chen Y, et al. An in situ cross-linked 1D/3D perovskite heterostructure improves the stability of hybrid perovskite solar cells for over 3000 h operation. *Energy Environ Sci*. 2020;13(11):4344-4352. b Kong T, Xie H, Zhang Y, et al. Perovskitoid-templated formation of a 1D@3D perovskite structure toward highly efficient and stable perovskite solar cells. *Advanced Energy Materials*. 2021;11(34):2101018.

17. Liu X, Li B, Zhang N, et al. Multifunctional RbCl dopants for efficient inverted planar perovskite solar cell with ultra-high fill factor, negligible hysteresis and improved stability. *Nano Energy*. 2018;53:567-578.

18. Weng H. Lighting up Weyl semimetals. *Nat Mater*. 2019;18: 428-429.

19. a Yan W, Ye S, Li Y, et al. Hole-transporting materials in inverted planar perovskite solar cells. *Adv Energy Mater*. 2016; 6(17):1600474. b Yin X, Song Z, Li Z, Tang W. Toward ideal hole transport materials: a review on recent progress in dopant-free hole transport materials for fabricating efficient and stable perovskite solar cells. *Energy Environ Sci*. 2020;13 (11):4057-4086. c Lin L, Jones TW, Yang TC-J, et al. Inorganic electron transport materials in perovskite solar cells. *Adv Funct Mater*. 2021;31(5):2008300. d) Lian J, Lu B, Niu F, Zeng P, Zhan X. Electron-transport materials in perovskite solar cells. *Small Methods*. 2018;2(10):1800082.

20. a Petridis C, Kakavelakis G, Kymakis E. Renaissance of graphene-related materials in photovoltaics due to the emergence of metal halide perovskite solar cells. *Energy Environ Sci*. 2018;11(5):1030-1061. b Haque MA, Sheikh AD, Guan X, Wu T. Metal oxides as efficient charge transporters in perovskite solar cells. *Adv Energy Mater*. 2017;7(20):1602803.

21. a Stolterfoht M, Caprioglio P, Wolff CM, et al. The impact of energy alignment and interfacial recombination on the internal and external open-circuit voltage of perovskite solar cells. *Energy Environ Sci*. 2019;12(9):2778-2788. b Liu Z, Krückemeier L, Krogmeier B, et al. Open-circuit voltages exceeding 1.26 v in planar methylammonium lead iodide perovskite solar cells. *ACS Energy Lett*. 2019;4(1):110-117. c Stranks SD, Hoye RLZ, Di D, Friend RH, Deschler F. The Physics of Light Emission in Halide Perovskite Devices. *Adv Mater*. 2019;31(47):e1803336.

22. Rau U. Reciprocity relation between photovoltaic quantum efficiency and electroluminescent emission of solar cells. *Phys Rev B*. 2007;76(8):085303.

23. Lan C, Dong R, Zhou Z, et al. Large-scale synthesis of freestanding layer-structured pbi_2 and $mapbi_3$ nanosheets for high-performance photodetection. *Adv Mater*. 2017;29(39):1702759.

24. Liu J, Xue Y, Wang Z, et al. Two-dimensional $CH_3NH_3PbI_3$ perovskite: synthesis and optoelectronic application. *ACS Nano*. 2016; 10(3):3536-3542.

25. Tian H, Zhao L, Wang X, et al. Extremely low operating current resistive memory based on exfoliated 2d perovskite single crystals for neuromorphic computing. *ACS Nano*. 2017;11(12): 12247-12256.

26. Ha ST, Liu X, Zhang Q, Giovanni D, Sum TC, Xiong Q. Synthesis of organic-inorganic lead halide perovskite nanoplatelets: towards high-performance perovskite solar cells and optoelectronic devices. *Adv Opt Mater*. 2014;2(9):838-844.

27. Schmidt LC, Pertegás A, González-Carrero S, et al. Nontemplate synthesis of $CH_3NH_3PbBr_3$ perovskite nanoparticles. *J Am Chem Soc*. 2014;136(3):850-853.

28. Parobek D, Dong Y, Qiao T, Son DH. Direct hot-injection synthesis of mn-doped CsPbBr3 nanocrystals. *Chem Mater*. 2018; 30(9):2939-2944.

29. Ma C, Shen D, Huang B, et al. High performance low-dimensional perovskite solar cells based on a one dimensional lead iodide perovskite. *J Mater Chem A*. 2019;7(15):8811-8817.

30. Lin H, Zhou C, Tian Y, Siegrist T, Ma B. Low-dimensional organometal halide perovskites. *ACS Energy Lett*. 2018;3(1):54-62.

31. Liu X, Zhang N, Tang B, et al. Highly stable new organic–inorganic hybrid 3D perovskite $CH_3NH_3PdI_3$ and 2D perovskite $(CH_3NH_3)_3Pd_2I_7$: DFT analysis, synthesis,

32. Liu X, Huang TJ, Zhang L, et al. Highly stable, new, organic-inorganic perovskite $(CH_3NH_3)_2PdBr_4$: Synthesis, structure, and physical properties. *Chem Eur J*. 2018;24(19):4991-4998.

33. Marongiu D, Saba M, Quochi F, Mura A, Bongiovanni G. The role of excitons in 3D and 2D lead halide perovskites. *J Mater Chem C*. 2019;7(39):12006-12018.

34. Yuan Z, Zhou C, Tian Y, et al. One-dimensional organic lead halide perovskites with efficient bluish white-light emission. *Nat Commun*. 2017;8:14051.

35. Hu T, Smith MD, Dohner ER, et al. Mechanism for broadband white-light emission from two-dimensional (110) hybrid perovskites. *J Phys Chem Lett*. 2016;7(12):2258-2263.

36. Kuang Y, Zhu C, He W, et al. Regulated exciton dynamics and optical properties of single perovskite CsPbBr$_3$ quantum dots by diluting surface ligands. *J Phys Chem C*. 2020;124(43): 23905-23912.

37. Tsai H, Nie W, Blancon J-C, et al. High-efficiency two-dimensional ruddlesden–popper perovskite solar cells. *Nature*. 2016;536:312-316.

38. Zhang D, Gu L, Zhang Q, et al. Increasing photoluminescence quantum yield by nanophotonic design of quantum-confined halide perovskite nanowire arrays. *Nano Lett*. 2019;19(5): 2850-2857.

39. Zheng K, Zhu Q, Abdellah M, et al. Exciton binding energy and the nature of emissive states in organometal halide perovskites. *J Phys Chem Lett*. 2015;6(15):2969-2975.

40. Peng H, Yao S, Guo Y, et al. Highly efficient self-trapped exciton emission of a $(MA)_4Cu_2Br_6$ single crystal. *J Phys Chem Lett*. 2020;11(12):4703-4710.

41. Zhang Y, Zhu H, Huang T, Song Z, Ruan S. Radiation-pressure-induced photoluminescence enhancement of all-inorganic perovskite CsPbBr$_3$ quantum dots. *Photonics Res*. 2019;8(7):1086-1092.

42. a) Yin Z, Leng J, Wang S, et al. Auger-assisted electron transfer between adjacent quantum wells in two-dimensional layered perovskites. *J Am Chem Soc*. 2021;143(12):4725-4731. b) Westbrook RJE, Xu W, Liang X, Webb T, Clarke TM, Haque SA. 2D Phase purity determines charge-transfer yield at 3d/2d lead halide perovskite heterojunctions. *J Phys Chem Lett*. 2021;12(13):3312-3320.

43. Sum TC, Mathews N, Xing G, et al. Spectral features and charge dynamics of lead halide perovskites: origins and interpretations. *Acc Chem Res*. 2016;49(2):294-302.

44. D'innocenzo V, Grancini G, Alcocer M, et al. Excitons versus free charges in organo-lead tri-halide perovskites. *Nat Commun*. 2014;5:3586.

45. Richter JM, Abdi-Jalebi M, Sadhanala A, et al. Enhancing photoluminescence yields in lead halide perovskites by photon recycling and light out-coupling. *Nat Commun*. 2016;7: 13941.

46. Shi J, Li Y, Li Y, et al. From ultrafast to ultraslow: charge-carrier dynamics of perovskite solar cells. *Joule*. 2018;2(5):879-901.

47. Pazos-Outón LM, Szumilo M, Lamboll R, et al. Photon recycling in lead iodide perovskite solar cells. *Science*. 2016; 351(6280):1430-1433.

48. a Liu X, Yu Z, Wang T, et al. Full defects passivation enables 21% efficiency perovskite solar cells operating in air. *Adv*

Energy Mater. 2020;10(38):2001958. b Cheng B, Li T-Y, Maity P, et al. Extremely reduced dielectric confinement in two-dimensional hybrid perovskites with large polar organics. *Commun Phys*. 2018;1:80. c Cui B-B, Han Y, Huang B, et al. Locally collective hydrogen bonding isolates lead octahedra for white emission improvement. *Nat Commun*. 2019;10:5190.

49. Richter JM, Branchi F, de Almeida Camargo FV, et al. Ultrafast carrier thermalization in lead iodide perovskite probed with two-dimensional electronic spectroscopy. *Nat Commun*. 2017; 8:376.

50. Yang Y, Ostrowski DP, France RM, et al. Observation of a hot-phonon bottleneck in lead-iodide perovskites. *Nat Photonics*. 2015;10:53-59.

51. Cho C, Zhao B, Tainter GD, et al. The role of photon recycling in perovskite light-emitting diodes. *Nat Commun*. 2020; 11:611.

52. Mandal S, Tkachenko NV. Multiphoton excitation of cspbbr3perovskite quantum dots (pqds): how many electrons can one pqd donate to multiple molecular acceptors? *J Phys Chem Lett*. 2019;10(11):2775-2781.

53. Mandal S, George L, Tkachenko NV. Charge transfer dynamics in $CsPbBr_3$ perovskite quantum dots–anthraquinone/fullerene (C60) hybrids. *Nanoscale*. 2019;11(3):862-869.

54. Qian J, Guo Q, Liu L, Xu B, Tian W. A theoretical study of hybrid lead iodide perovskite homologous semiconductors with 0D, 1D, 2D and 3D structures. *J Mater Chem A*. 2017;5 (32):16786-16795.

55. Liu P, Xian Y, Yuan W, et al. Lattice-matching structurally-stable 1D@3D perovskites toward highly efficient and stable solar cells. *Adv Energy Mater*. 2020;10(17):1903654.

56. Wang HC, Bao Z, Tsai HY, Tang AC, Liu RS. Perovskite quantum dots and their application in light-emitting diodes. *Small*. 2018;14(1):1702433.

57. a Zhao Y, Zhu P, Wang M, et al. A Polymerization-assisted grain growth strategy for efficient and stable perovskite solar cells. *Advanced Materials*. 2020;32(17):1907769. b Yang S, Chen S, Mosconi E, et al. Stabilizing halide perovskite surfaces for solar cell operation with wide-bandgap lead oxysalts. *Science*. 2019;365(6452):473-478.

58. Lin K, Xing J, Quan LN, et al. Perovskite light-emitting diodes with external quantum efficiency exceeding 20 per cent. *Nature*. 2018;562:245-248.

59. Cao Y, Wang N, Tian H, et al. Perovskite light-emitting diodes based on spontaneously formed submicrometre-scale structures. *Nature*. 2018;562:249-253.

60. Xu W, Hu Q, Bai S, et al. Rational molecular passivation for high-performance perovskite light-emitting diodes. *Nat Photonics*. 2019;13:418-424.

61. Ortiz-Cervantes C, Carmona-Monroy P, Solis-Ibarra D. Two-Dimensional halide perovskites in solar cells: 2d or not 2d? *ChemSusChem*. 2019;12(8):1560-1575.

62. Hu JYan L, You W. Two-dimensional organic–inorganic hybrid perovskites: a new platform for optoelectronic applications. *Adv Mater*. 2018;30(48):e1802041.

63. Liu W, Xing J, Zhao J, et al. Giant two-photon absorption and its saturation in 2d organic-inorganic perovskite. *Adv Opt Mater*. 2017;5(7):1601045.

64. Zhao Y-Q, Ma Q-R, Liu B, Yu Z-L, Yang J, Cai M-Q. Layer-dependent transport and optoelectronic property in two-dimensional perovskite: $(PEA)_2PbI_4$. *Nanoscale*. 2018;10(18): 8677-8688.

65. Dou LT, Wong AB, Yu Y, et al. Atomically thin two-dimensional organic-inorganic hybrid perovskites. *Science*. 2015;349(6255):1518-1521.

66. Kim YH, Kim JS, Lee TW. Strategies to improve luminescence efficiency of metal-halide perovskites and light-emitting diodes. *Adv Mater*. 2019;31(47):e1804595.

67. Zhai Y, Baniya S, Zhang C, et al. Giant Rashba splitting in 2D organic-inorganic halide perovskites measured by transient spectroscopies. *Sci Adv*. 2017;3:e1700704.

68. Liu Y, Ye H, Zhang Y, et al. Surface-tension-controlled crystallization for high-quality 2D perovskite single crystals for ultrahigh photodetection. *Matter*. 2019;1(2):465-480.

69. Im JH, Luo J, Franckevicius M, et al. Nanowire Perovskite Solar Cell. *Nano Lett*. 2015;15(3):2120-2126.

70. a Wang S, Yan S, Wang M, Chang L, Wang J, Wang Z. Construction of nanowire $CH_3NH_3PbI_3$ -based solar cells with 17.62% efficiency by solvent etching technique. *Sol Energy Mater Sol Cells*. 2017;167:173-177. b Singh R, Suranagi SR, Yang SJ, Cho K. Enhancing the power conversion efficiency of perovskite solar cells via the controlled growth of perovskite nanowires. *Nano Energy*. 2018;51:192-198.

71. Chang C-Y, Tsai B-C, Lin M-Z, Huang Y-C, Tsao C-S. An integrated approach towards the fabrication of highly efficient and long-term stable perovskite nanowire solar cells. *J Mater Chem A*. 2017;5(43):22824-22833.

72. Swarnkar A, Marshall AR, Sanehira EM, et al. Quantum dot-induced phase stabilization of -CsPbI_3 perovskite for high-efficiency photovoltaics. *Science*. 2016;354(6308):92-95.

73. Sanehira EM, Marshall AR, Christians JA, et al. Enhanced mobility $CsPbI_3$ quantum dot arrays for record-efficiency, high-voltage photovoltaic cells. *Sci Adv*. 2017;3:eaao4204.

74. Ren H, Yu S, Chao L, et al. Efficient and stable Ruddlesden–Popper perovskite solar cell with tailored interlayer molecular interaction. *Nat Photonics*. 2020;14:154-163.

75. Kubicki DJ, Prochowicz D, Hofstetter A, et al. Cation dynamics in mixed-cation $(MA)_x(FA)_{1-x}PbI_3$ Hybrid Perovskites from Solid-State NMR. *J Am Chem Soc*. 2017;139 (29):10055-10061.

76. Zhang F, Zhong H, Chen C, et al. Brightly Luminescent and Color-Tunable Colloidal $CH_3NH_3PbX_3(X = Br, I, Cl)$ Quantum Dots: Potential Alternatives for Display Technology. *ACS Nano*. 2015;9(4):4533-4542.

77. Wang Y, Li X, Song J, Xiao L, Zeng H, Sun H. All-inorganic colloidal perovskite quantum dots: a new class of lasing materials with favorable characteristics. *Adv Mater*. 2015;27(44):7101-7108.

78. Protesescu L, Yakunin S, Bodnarchuk MI, et al. Nanocrystals of cesium lead halide perovskites ($CsPbX_3$, X = Cl, Br, and I): Novel optoelectronic materials showing bright emission with wide color gamut. *Nano Lett*. 2015;15(6):3692-3696.

79. Song J, Li J, Li X, Xu L, Dong Y, Zeng H. Quantum dot light-emitting diodes based on inorganic perovskite cesium lead halides ($CsPbX_3$). *Adv Mater*. 2015;27(44):7162-7167.

80. a Li J, Xu L, Wang T, et al. 50-Fold eqe improvement up to 6.27% of solution-processed all-inorganic perovskite $CsPbBr_3$QLEDs via surface ligand density control. *Adv Mater*. 2017;29(5):1603885. b Zou S, Liu Y, Li J, et al. Stabilizing cesium lead halide perovskite lattice through mn(ii) substitution for air-stable light-emitting

diodes. *J Am Chem Soc.* 2017;139(33):11443-11450. c Chen W, Tang X, Wangyang P, et al. Surface-passivated cesium lead halide perovskite quantum dots: toward efficient light-emitting diodes with an inverted sandwich structure. *Adv Opt Mater.* 2018;6(14): 1800007.

81. Chiba T, Hayashi Y, Ebe H, et al. Anion-exchange red perovskite quantum dots with ammonium iodine salts for highly efficient light-emitting devices. *Nat Photonics.* 2018;12:681-687.

82. a Prasanna R, Gold-Parker A, Leijtens T, et al. Band gap tuning via lattice contraction and octahedral tilting in perovskite materials for photovoltaics. *J Am Chem Soc.* 2017;139(32): 11117-11124. b Unger EL, Kegelmann L, Suchan K, Sörell D, Korte L, Albrecht S. Roadmap and roadblocks for the band gap tunability of metal halide perovskites. *J Mater Chem A.* 2017;5(23):11401-11409.

83. He T, Jiang Y, Xing X, Yuan M. Structured perovskite light absorbers for efficient and stable photovoltaics. *Adv Mater.* 2020;32:1903937.

84. Miao Y, Chen Y, Chen H, Wang X, Zhao Y. Using steric hindrance to manipulate and stabilize metal halide perovskites for optoelectronics. *Chem Sci.* 2021;12(21):7231-7247.

85. Cao DH, Stoumpos CC, Farha OK, Hupp JT, Kanatzidis MG. 2D Homologous Perovskites as Light-Absorbing materials for solar cell applications. *J Am Chem Soc.* 2015;137(24):7843-7850.

86. Stoumpos CC, Cao DH, Clark DJ, et al. Ruddlesden–popper hybrid lead iodide perovskite 2D homologous semiconductors. *Chem Mater.* 2016;28(8):2852-2867.

87. Smith IC, Hoke ET, Solis-Ibarra D, McGehee MD, Karunadasa HI. A layered hybrid perovskite solar-cell absorber with enhanced moisture stability. *Angew Chem Int Ed Engl.* 2014;53(42):11232-11235.

88. Chen AZ, Shiu M, Ma JH, et al. Origin of vertical orientation in two-dimensional metal halide perovskites and its effect on photovoltaic performance. *Nat Commun.* 2018;9:1336.

89. Quan LN, Yuan M, Comin R, et al. Ligand-stabilized reduced-dimensionality perovskites. *J Am Chem Soc.* 2016;138(8):2649-2655.

90. Yang R, Li R, Cao Y, et al. Oriented quasi-2D perovskites for high performance optoelectronic devices. *Adv Mater.* 2018;30 (51):e1804771.

91. Wu G, Zhou J, Zhang J, et al. Management of the crystallization in two-dimensional perovskite solar cells with enhanced efficiency within a wide temperature range and high stability. *Nano Energy.* 2019;58:706-714.

92. Lai H, Kan B, Liu T, et al. Two-dimensional ruddlesden–popper perovskite with nanorod-like morphology for solar cells with efficiency exceeding 15%. *J Am Chem Soc.* 2018;140 (37):11639-11646.

93. Li X, Wu G, Zhou J, et al. Non-preheating processed quasi-2D perovskites for efficient and stable solar cells. *Small.* 2020;16: e1906997.

94. Tsai H, Asadpour R, Blancon JC, et al. Design principles for electronic charge transport in solution-processed vertically stacked 2D perovskite quantum wells. *Nat Commun.* 2018;9:2130.

95. a Zhang X, Ren X, Liu B, et al. Stable high efficiency two-dimensional perovskite solar cells via cesium doping. *Energy Environ Sci.* 2017;10(10):2095-2102. b Zhou N, Shen Y, Li L, et al. Exploration of crystallization kinetics in quasi two-dimensional perovskite and high performance solar cells. *J Am Chem Soc.* 2018;140(1):459-465.

96. Gao L, Zhang F, Chen X, et al. Enhanced charge transport by incorporating formamidinium and cesium cations into two-dimensional perovskite solar cells. *Angew Chem Int Ed Engl.* 2019;58(34):11737-11741.

97. Zhou NHuang B, Sun M, et al. The spacer cations interplay for efficient and stable layered 2D Perovskite Solar Cells. *Adv Energy Mater.* 2019;10(1):1901566.

98. Mao L, Stoumpos CC, Kanatzidis MG. Two-dimensional hybrid halide perovskites: principles and promises. *J Am Chem Soc.* 2019;141(3):1171-1190.

99. Yuan M, Quan LN, Comin R, et al. Perovskite energy funnels for efficient light-emitting diodes. *Nat Nanotechnol.* 2016;11:872-877.

100. Zhao B, Bai S, Kim V, et al. High-efficiency perovskite–polymer bulk heterostructure light-emitting diodes. *Nat Photonics.* 2018;12:783-789.

101. Lei L, Seyitliyev D, Stuard S, et al. Efficient energy funneling in quasi-2D perovskites: from light emission to lasing. *Adv Mater.* 2020;32:e1906571.

102. Meng F, Liu X, Chen Y, et al. Co-interlayer engineering toward efficient green quasi-two-dimensional perovskite light-emitting diodes. *Adv Funct Mater.* 2020;30:1910167.

103. Zhao B, Lian Y, Cui L, et al. Efficient light-emitting diodes from mixed-dimensional perovskites on a fluoride interface. *Nat Electronics.* 2020;3:704-710.

104. Ema K, Inomata M, Kato Y, Kunugita H, Era M. Nearly perfect triplet-triplet energy transfer from wannier excitons to naphthalene in organic-inorganic hybrid quantum-well materials. *Phys Rev Lett.* 2008;100:257401.

105. Vashishtha P, Ng M, Shivarudraiah SB, Halpert JE. High efficiency blue and green light-emitting diodes using ruddlesden–popper inorganic mixed halide perovskites with butylammonium interlayers. *Chem Mater.* 2019;31(1):83-89.

106. Qin C, Matsushima T, Potscavage WJ, et al. Triplet management for efficient perovskite light-emitting diodes. *Nat Photonics.* 2019;14:70-75.

107. Jiang Y, Qin C, Cui M, et al. Spectra stable blue perovskite light-emitting diodes. *Nat Commun.* 2019;10:1868.

108. Li Z, Chen Z, Yang Y, Xue Q, Yip HL, Cao Y. Modulation of recombination zone position for quasi-two-dimensional blue perovskite light-emitting diodes with efficiency exceeding 5%. *Nat Commun.* 2019;10:1027.

109. Wang YK, Ma D, Yuan F, et al. Chelating-agent-assisted control of CsPbBr3 quantum well growth enables stable blue perovskite emitters. *Nat Commun.* 2020;11:3674.

110. Chu Z, Zhao Y, Ma F, et al. Large cation ethylammonium incorporated perovskite for efficient and spectra stable blue light-emitting diodes. *Nat Commun.* 2020;11:4165.

111. Ma D, Todorovic P, Meshkat S, et al. Chloride insertion–immobilization enables bright, narrowband, and stable blue-emitting perovskite diodes. *J Am Chem Soc.* 2020;142(11): 5126-5134.

112. a Cohen B-E, Wierzbowska M, Etgar L. High efficiency quasi 2D lead bromide perovskite solar cells using various barrier molecules. *Sustainable Energy Fuels.* 2017;1(9):1935-1943. b Zhou M, Fei C, Sarmiento JS, Wang H. Manipulating the phase distributions and carrier transfers in hybrid quasi-two-dimensional perovskite films. *Solar RRL.* 2019;3(4):1800359.

113. Tai M, Zhou Y, Yin X, et al. In situ formation of a 2D/3D heterostructure for efficient and stable CsPbI$_2$Br solar cells. *J Mater Chem A*. 2019;7(39):22675-22682.

114. Hu J, Wang C, Qiu S, et al. Spontaneously self-assembly of a 2D/3D heterostructure enhances the efficiency and stability in printed perovskite solar cells. *Adv Energy Mater*. 2020;10:2000173.

115. Hu Y, Schlipf J, Wussler M, et al. Hybrid perovskite/perovskite heterojunction solar cells. *ACS Nano*. 2016;10(6):5999-6007.

116. Abbas MS, Hussain S, Zhang J, et al. Orientationally engineered 2D/3D perovskite for high efficiency solar cells. *Sustainable Energy Fuels*. 2020;4(1):324-330.

117. Chen P, Meng Y, Ahmadi M, et al. Charge-transfer versus energy-transfer in quasi-2D perovskite light-emitting diodes. *Nano Energy*. 2018;50:615-622.

118. Cho KT, Grancini G, Lee Y, et al. Selective growth of layered perovskites for stable and efficient photovoltaics. *Energy Environ Sci*. 2018;11(4):952-959.

119. Gharibzadeh S, Abdollahi Nejand B, Jakoby M, et al. Record open-circuit voltage wide-bandgap perovskite solar cells utilizing 2D/3D perovskite heterostructure. *Adv Energy Mater*. 2019;9:1803699.

120. Proppe AH, Wei M, Chen B, Quintero-Bermudez R, Kelley SO, Sargent EH. Photochemically cross-linked quantum well ligands for 2D/3D perovskite photovoltaics with improved photovoltage and stability. *J Am Chem Soc*. 2019;141(36):14180-14189.

121. Wang Z, Lin Q, Chmiel FP, Sakai N, Herz LM, Snaith HJ. Efficient ambient-air-stable solar cells with 2D–3D heterostructured butylammonium-caesium-formamidinium lead halide perovskites. *Nat Energy*. 2017;2:17135.

122. Buizza LRV, Crothers TW, Wang Z, et al. Charge-carrier dynamics, mobilities, and diffusion lengths of 2D–3D hybrid butylammonium–cesium–formamidinium lead halide perovskites. *Adv Funct Mater*. 2019;29:1902656.

123. Niu T, Lu J, Tang M-C, et al. High performance ambient-air-stable FAPbI$_3$ perovskite solar cells with molecule-passivated Ruddlesden–Popper/3D heterostructured film. *Energy Environ Sci*. 2018;11(12):3358-3366.

124. Lee JW, Dai Z, Han TH, et al. 2D perovskite stabilized phase-pure formamidinium perovskite solar cells. *Nat Commun*. 2018;9:3021.

125. Hu Y, Qiu T, Bai F, Ruan W, Zhang S. Highly Efficient and Stable Solar Cells with 2D MA$_3$Bi$_2$I$_9$/3D MAPbI$_3$ heterostructured Perovskites. *Adv Energy Mater*. 2018;8:1703620.

126. Wang F, Jiang X, Chen H, et al. 2D-Quasi-2D-3D Hierarchy structure for tin perovskite solar cells with enhanced efficiency and stability. *Joule*. 2018;2(12):2732-2743.

127. Han T-H, Lee J-W, Choi YJ, et al. Surface-2D/bulk-3D heterophased perovskite nanograins for long-term-stable light-emitting diodes. *Adv Mater*. 2020;32:1905674.

128. Zhang F, Cai B, Song J, Han B, Zhang B, Zeng H. Efficient blue perovskite light-emitting diodes boosted by 2D/3D energy cascade channels. *Adv Funct Mater*. 2020;30:2001732.

129. a Liu M, Chen Y, Tan CS, et al. Lattice anchoring stabilizes solution-processed semiconductors. *Nature*. 2019;570:96-101. b Li S-S, Chang C-H, Wang Y-C, et al. Intermixing-seeded growth for high-performance planar heterojunction perovskite solar cells assisted by precursor-capped nanoparticles. *Energy Environ Sci*. 2016;9(4):1282-1289. c Gao L, Quan LN, García de Arquer FP, et al. Efficient near-infrared light-emitting diodes

based on quantum dots in layered perovskite. *Nat Photonics*. 2020;14:227-233. d Ning Z, Gong X, Comin R, et al. Quantum-dot-in-perovskite solids. *Nature*. 2015;523:324-328.

130. Wang X, Ling Y, Lian X, et al. Suppressed phase separation of mixed-halide perovskites confined in endotaxial matrices. *Nat Commun*. 2019;10:695.

131. Bai F, Zhang J, Yuan Y, et al. A 0D/3D Heterostructured all-inorganic halide perovskite solar cell with high performance and enhanced phase stability. *Adv Mater*. 2019;31(48):e1904735.

132. Zheng X, Troughton J, Gasparini N, et al. Quantum dots supply bulk- and surface-passivation agents for efficient and stable perovskite solar cells. *Joule*. 2019;3(8):1963-1976.

133. Xie L, Vashishtha P, Koh TM, et al. Realizing reduced imperfections via quantum dots interdiffusion in high efficiency perovskite solar cells. *Adv Mater*. 2020;32(40):e2003296.

134. Yang W, Su R, Luo D, et al. Surface modification induced by perovskite quantum dots for triple-cation perovskite solar cells. *Nano Energy*. 2020;67:104189.

135. Zhang J, Bai D, Jin Z, et al. 3D-2D-0D Interface profiling for record efficiency all-inorganic CsPbBrI$_2$ perovskite solar cells with superior stability. *Adv Energy Mater*. 2018;8:1703246.

136. Zhao Q, Hazarika A, Chen X, et al. High efficiency perovskite quantum dot solar cells with charge separating heterostructure. *Nat Commun*. 2019;10:2842.

137. Gao L, Spanopoulos I, Ke W, et al. Improved environmental stability and solar cell efficiency of (MA,FA)PbI$_3$ perovskite using a wide-band-gap 1D thiazolium lead iodide capping layer strategy. *ACS Energy Lett*. 2019;4(7):1763-1769.

138. Fan J, Ma Y, Zhang C, et al. Thermodynamically self-healing 1D-3D hybrid perovskite solar cells. *Adv Energy Mater*. 2018;8:1703421.

139. Niu T, Lu J, Jia X, et al. Interfacial engineering at the 2D/3D heterojunction for high-performance perovskite solar cells. *Nano Lett*. 2019;19(10):7181-7190.

140. Zheng X, Troughton J, Gasparini N, et al. Quantum dots supply bulk- and surface-passivation agents for efficient and stable perovskite solar cells. *Joule*. 2019;3(8):1963-1976.

141. Xie L, Vashishtha P, Koh TM, et al. Realizing reduced imperfections via quantum dots interdiffusion in high efficiency perovskite solar cells. *Adv Mater*. 2020;32:2003296.

142. Vasilopoulou M, Kim HP, Kim BS, et al. Efficient colloidal quantum dot light-emitting diodes operating in the second near-infrared biological window. *Nat Photonics*. 2019;14:50-56.

143. Chin XY, Perumal A, Bruno A, et al. Self-assembled hierarchical nanostructured perovskites enable highly efficient LED sviaan energy cascade. *Energy Environ Sci*. 2018;11(7):1770-1778.

144. Liu Y, Cui J, Du K, et al. Efficient blue light-emitting diodes based on quantum-confined bromide perovskite nanostructures. *Nat Photonics*. 2019;13:760-764.

145. Na Quan L, Ma D, Zhao Y, et al. Edge stabilization in reduced-dimensional perovskites. *Nat Commun*. 2020;11:170.

146. Tsai H, Liu C, Kinigstein E, et al. Critical role of organic spacers for bright 2D layered perovskites light-emitting diodes. *Adv Sci*. 2020;7:1903202.

147. Fakharuddin A, Qiu W, Croes G, et al. Reduced efficiency roll-off and improved stability of mixed 2D/3D perovskite

light emitting diodes by balancing charge injection. *Adv Funct Mater*. 2019;29:1904101.

148. Ghosh D, Chaudhary DK, Ali MY, et al. All-inorganic quantum dot assisted enhanced charge extraction across the interfaces of bulk organo-halide perovskites for efficient and stable pin-hole free perovskite solar cells. *Chem Sci*. 2019;10 (41):9530-9541.

149. Li Z, Liu X, Xu J, et al. All-inorganic 0D/3D $Cs_4Pb(IBr)_6$ /$CsPbI_{3-x}Brx$ mixed-dimensional perovskite solar cells with enhanced efficiency and stability. *J Mater Chem C*. 2020;8(21): 6977-6987.

150. Peng Z, Wei Q, Chen H, et al. $Cs_{0.15}FA_{0.85}PbI_3$/$CsxFA_{1-x}PbI_3$ Core/shell heterostructure for highly stable and efficient perovskite solar cells. *Cell Rep Phys Sci*. 2020;1:100224.

151. Cheng Y, Xie C, Liu X, et al. High-power bifacial perovskite solar cells with shelf life of over 2000h. *Sci Bull*. 2020;65(8):607-610.

152. Hailegnaw B, Kirmayer S, Edri E, Hodes G, Cahen D. Rain on methylammonium lead iodide based perovskites: possible environmental effects of perovskite solar cells. *J Phys Chem Lett*. 2015;6(9):1543-1547.

153. Shi Z, Guo J, Chen Y, et al. Lead-free organic-inorganic hybrid perovskites for photovoltaic applications: recent advances and perspectives. *Adv Mater*. 2017;29:1605005.

154. Jiang Y, Qiu L, Juarez-Perez EJ, et al. Reduction of lead leakage from damaged lead halide perovskite solar modules using self-healing polymer-based encapsulation. *Nat Energy*. 2019;4: 585-593.

155. Li X, Zhang F, He H, Berry JJ, Zhu K, Xu T. On-device lead sequestration for perovskite solar cells. *Nature*. 2020;578:555-558.

156. Hu H, Dong B, Zhang W. Low-toxic metal halide perovskites: opportunities and future challenges. *J Mater Chem A*. 2017;5 (23):11436-11449.

157. Huang J, Tan S, Lund PD, Zhou H. Impact of H_2O on organic–inorganic hybrid perovskite solar cells. *Energy Environ Sci*. 2017;10(11):2284-2311.

158. Ye J, Zheng H, Zhu L, et al. Enhanced moisture stability of perovskite solar cells with mixed-dimensional and mixed-compositional light-absorbing materials. *Solar RRL*. 2017;1: 1700125.

159. Cheng Y, So F, Tsang S-W. Progress in air-processed perovskite solar cells: from crystallization to photovoltaic performance. *Mater Horiz*. 2019;6(8):1611-1624.

160. Zhou H, Chen Q, Li G, et al. Interface engineering of highly efficient perovskite solar cells. *Science*. 2014;345(6196):542-546.

161. Liu Z, Zheng H, Liu D, et al. Controllable two-dimensional perovskite crystallization via water additive for high-performance solar cells. *Nanoscale Res Lett*. 2020;15:108.

162. Gong X, Li M, Shi X-B, Ma H, Wang Z-K, Liao L-S. Controllable perovskite crystallization by water additive for high-performance solar cells. *Adv Funct Mater*. 2015;25(42):6671-6678.

163. Turedi B, Lee KJ, Dursun I, et al. Water-induced dimensionality reduction in metal-halide perovskites. *J Phys Chem C*. 2018;122(25):14128-14134.

164. Kim M, Kim JH, Kim M, et al. Enhanced photoluminescence quantum efficiency and stability of water assisted $CsPbBr_3$ perovskite nanocrystals. *J Ind Eng Chem*. 2020;88:84-89.

165. a Boyd CC, Cheacharoen R, Leijtens T, McGehee MD. Understanding degradation mechanisms and improving stability of perovskite photovoltaics. *Chem Rev*. 2019;119(5):3418-3451. b Bisquert J, Juarez-Perez EJ. The Causes of Degradation of Perovskite Solar Cells. *J Phys Chem Lett*. 2019;10(19):5889-5891.

166. a Cheng Y, Yang Q-D, Ding L. Encapsulation for perovskite solar cells. *Sci Bull*. 2021;66(2):100-102. b Lu Q, Yang Z, Meng X, et al. A review on encapsulation technology from organic light emitting diodes to organic and perovskite solar cells. *Adv Funct Mater*. 2021;31(23):2100151.

AUTHOR BIOGRAPHIES

Xixia Liu obtained his doctoral degree from Department of Materials Science and Engineering (MSE) at National University of Singapore (NUS) in 2020. Then he joined in Peking University as a national research associate and Huawei as a senior engineer sequentially. He is experienced in semiconductor simulation, device fabrications and characterizations, including solar cells, LEDs, photo-detectors, and emerging memories. Currently, he has published 24 SCI papers on Science, Energy & Environmental Science, Advanced Materials, Advanced Energy Materials, Nano Energy, etc. and has been granted 5 Chinese patents.
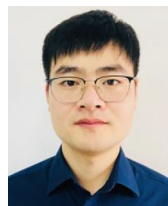
Yuanhang Cheng received his PhD degree from the Department of Physics and Materials Science, City University of Hong Kong, in October 2017. He is currently working as a Senior Research Fellow at the Solar Energy Research Institute of Singapore (SERIS), National University of Singapore. His research interests include perovskite solar cells, highly efficient perovskite/Si tandem solar cells, and new photovoltaic materials with various organic–inorganic composites.